Supporting Information

*Aistė Jegorovė,[a] Maryte Daskeviciene,[a] Kristina Kantminienė,[b] Vygintas Jankauskas,[c] Romualdas Jonas Čepas,[c] Alytis Gruodis,[c] Vytautas Getautis[a] and Kristijonas Genevičius[c]**

[a] Department of Organic Chemistry, Kaunas University of Technology, Radvilėnų pl. 19, Kaunas, 50254 Lithuania

[b] Department of Physical and Inorganic Chemistry, Kaunas University of Technology, Radvilėnų pl. 19, Kaunas, 50254 Lithuania

[c] Institute of Chemical Physics, Vilnius University, Saulėtekio al. 3, Vilnius 10257, Lithuania

Materials

2-Ethylhexylbromide, Silicagel (230–400 mesh, 60 Å), palladium (II) acetate, 2-(dicyclohexylphosphino)-2',4',6'-triisopropyl-1,1'-biphenyl (XPhos), *tri-tert*-butylphosphonium tetrafluoroborate, 3-bromo-9*H*-carbazole, malononitrile, and triethylamine were supplied from Sigma-Aldrich. Potassium *tert*-butoxide (k-OtBu), 2-aminoanthracene-9,10-dione, sodium *tert*-butoxide (Na-OtBu), and 2-aminofluorenone were purchased from TCI Europe N. V.. *n*-Hexane, dioxane, ethylacetate, tetrahydrofuran (THF), acetone, toluene, methanol (MeOH), potassium hydroxide (KOH), sodium sulphate (Na_2SO_4), and acetic acid were purchased from Eurochemicals. Ethanol (EtOH) was purchased from "Vilniaus degtinė ". All commercial chemicals were used as received without further purification.

General methods

3-Bromo-9-(2-ethylhexyl)-9*H*-carbazole was synthesized as previously reported. [1] Its spectral data were in agreement with the reported values.

^{1}H NMR spectra were recorded at 400 MHz on a Bruker Avance III spectrometer, ^{13}C NMR spectra were collected using the same instrument at 101 MHz. The chemical shifts, expressed in ppm, were relative to tetramethylsilane (TMS). All the experiments were performed at 25 °C. Reactions were monitored by thin-layer chromatography on ALUGRAM SIL G/UV254 plates and developed under UV light. Silica gel (grade 9385, 230–400 mesh, 60 Å) was used for column chromatography.

Elemental analysis was performed on an Exeter Analytical CE-440 elemental analyzer, Model 440 C/H/N.

The transformations of thermal changes of target compounds were recorded with a TA Instruments Q2000 differential scanning calorimeter in a nitrogen atmosphere. From the obtained thermal curves, the glass transition temperatures of the materials were determined.

Heating and cooling mode was 10 °C/min. The destruction temperatures of the new compounds were recorded by TA Instruments Q50 by thermogravimetric analysis in a nitrogen atmosphere. The decomposition temperatures of compounds were recorded when the weight loss was 5%. Heating mode was 20 °C/min.

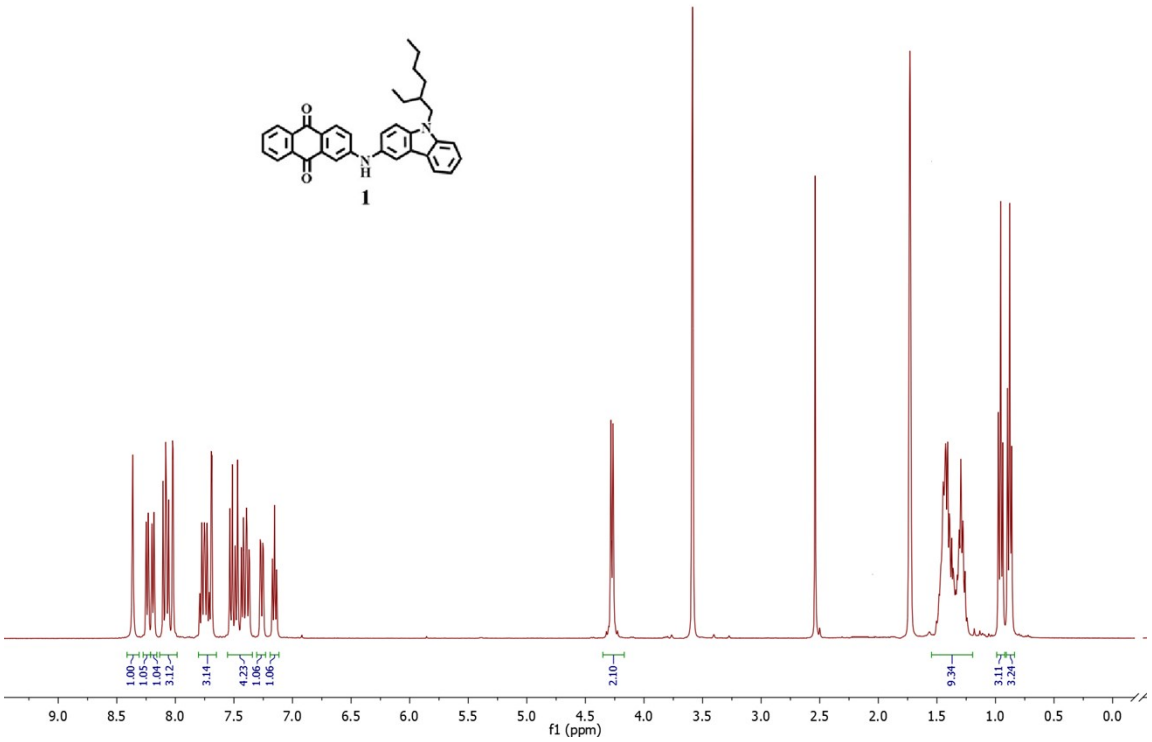

Figure S. 1 ^{1}H NMR spectra of intermediate **1**.

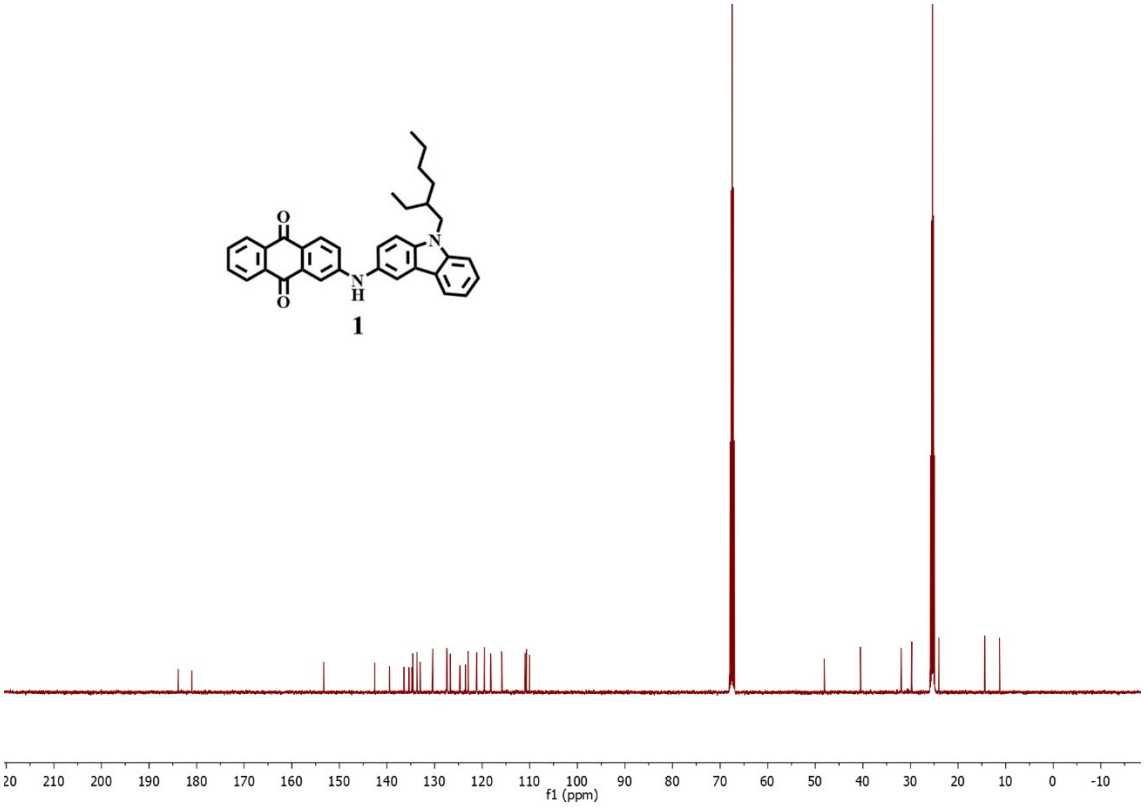

Figure S. 2 ^{13}C NMR spectra of intermediate **1**.

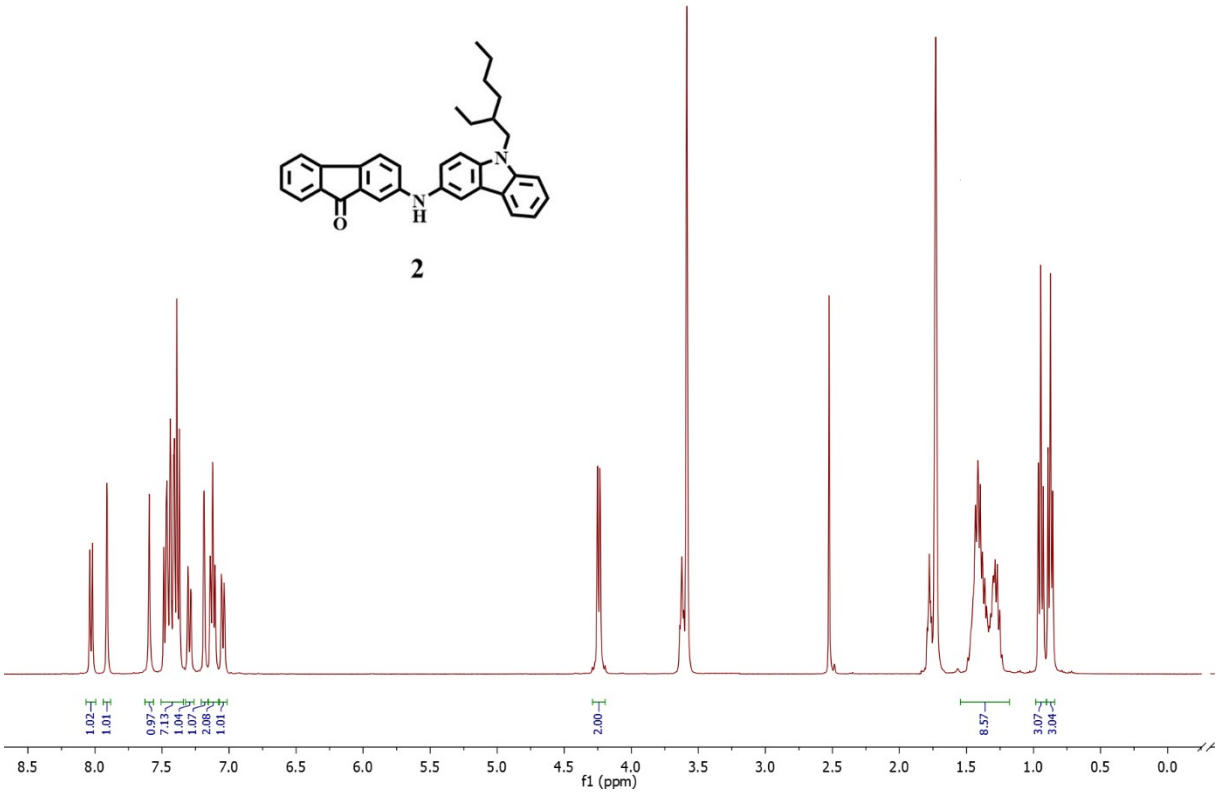

Figure S. 3 ^{1}H NMR spectra of intermediate **2**.

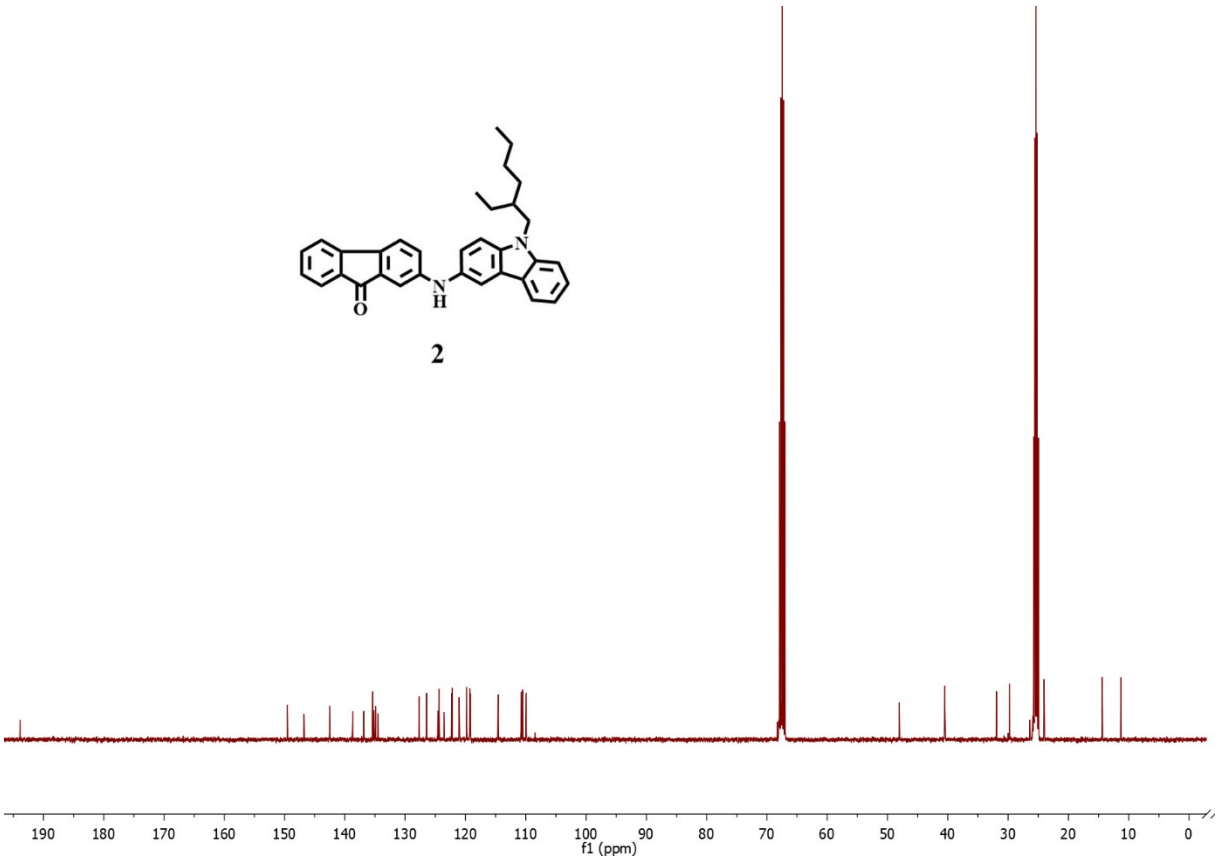

Figure S. 4 ^{13}C NMR spectra of intermediate **2**.

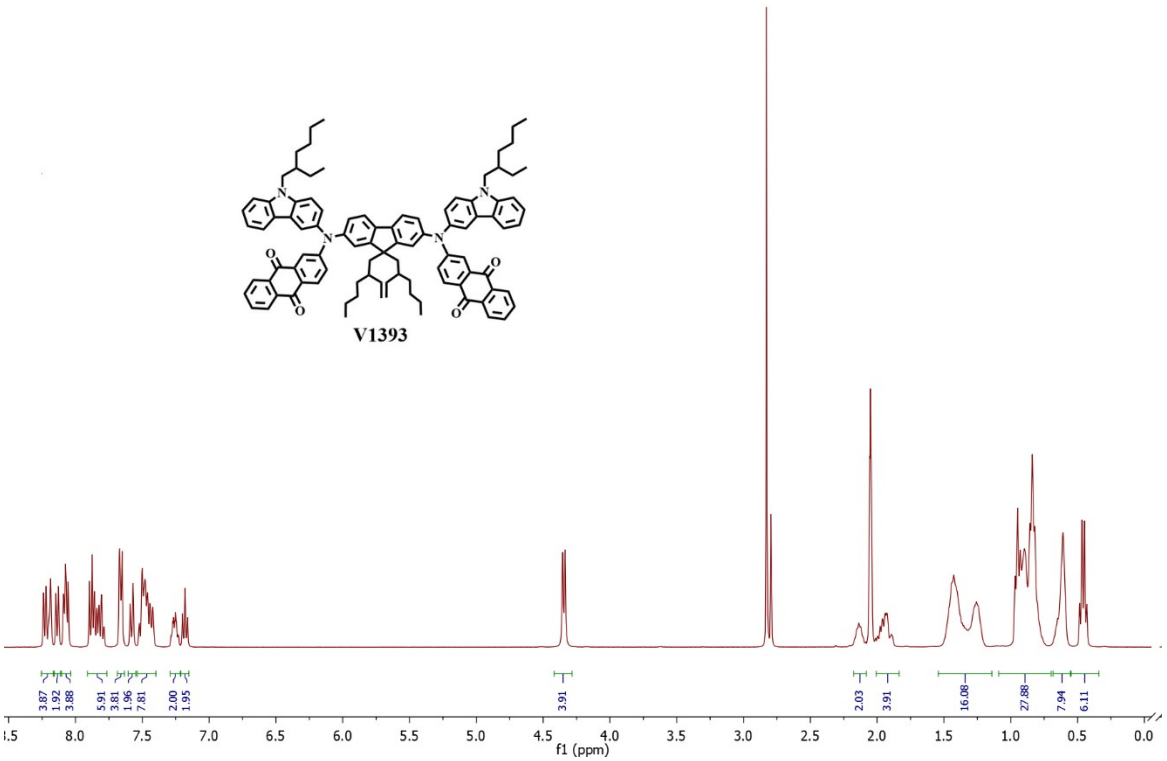

Figure S. 5 ^{1}H NMR spectra of target compound **V1393**.

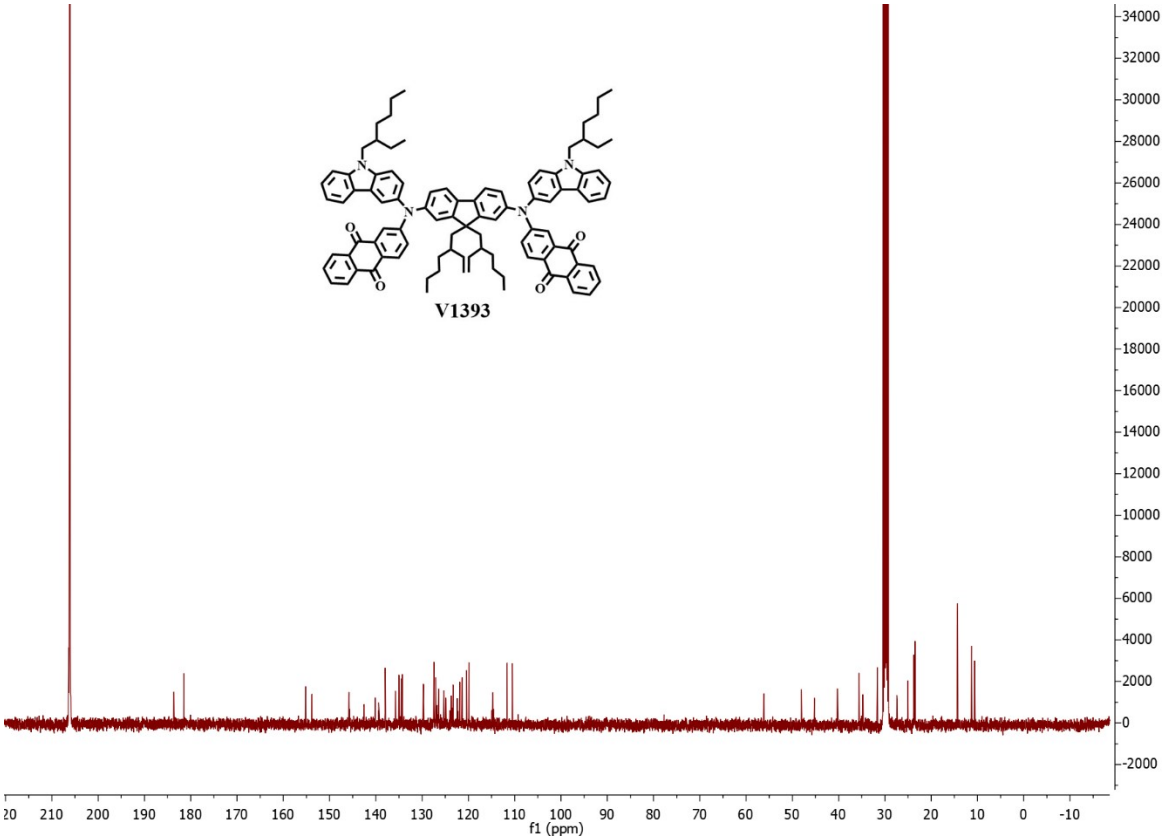

Figure S. 6 ^{13}C NMR spectra of target compound **V1393**.

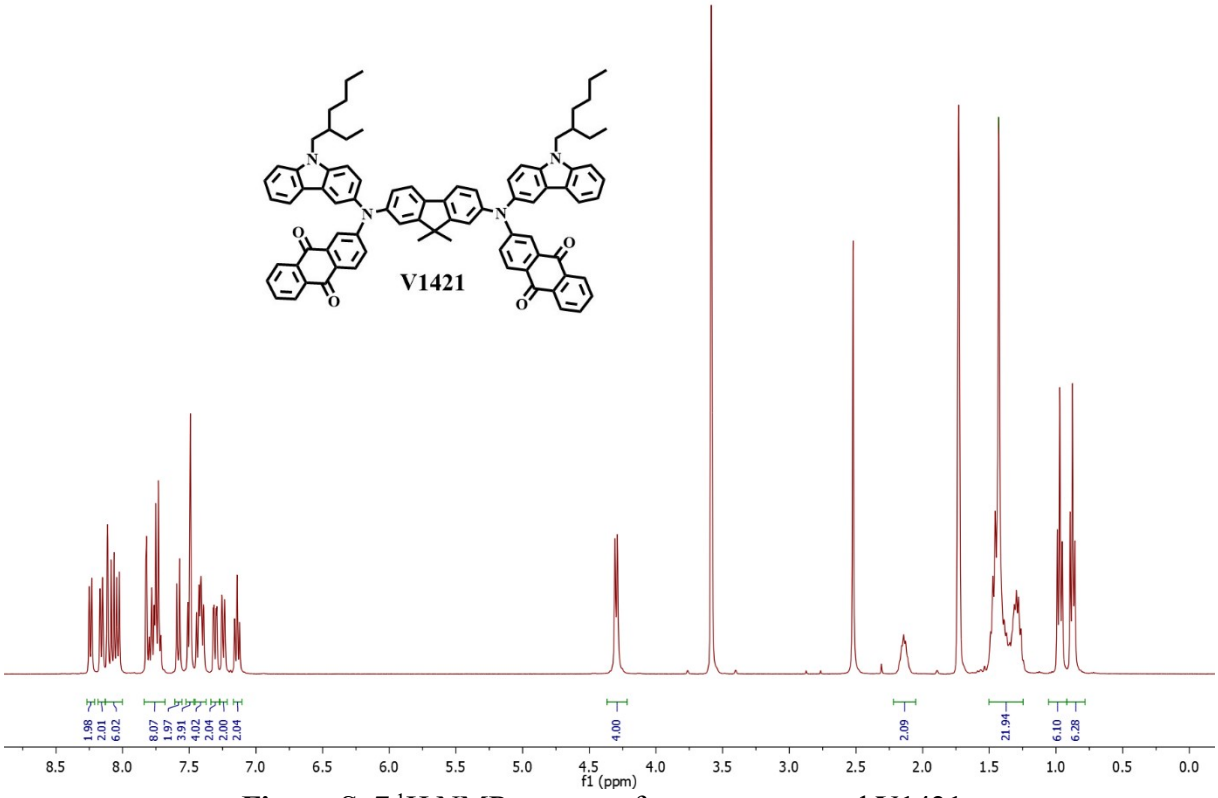

Figure S. 7 ^{1}H NMR spectra of target compound **V1421**.

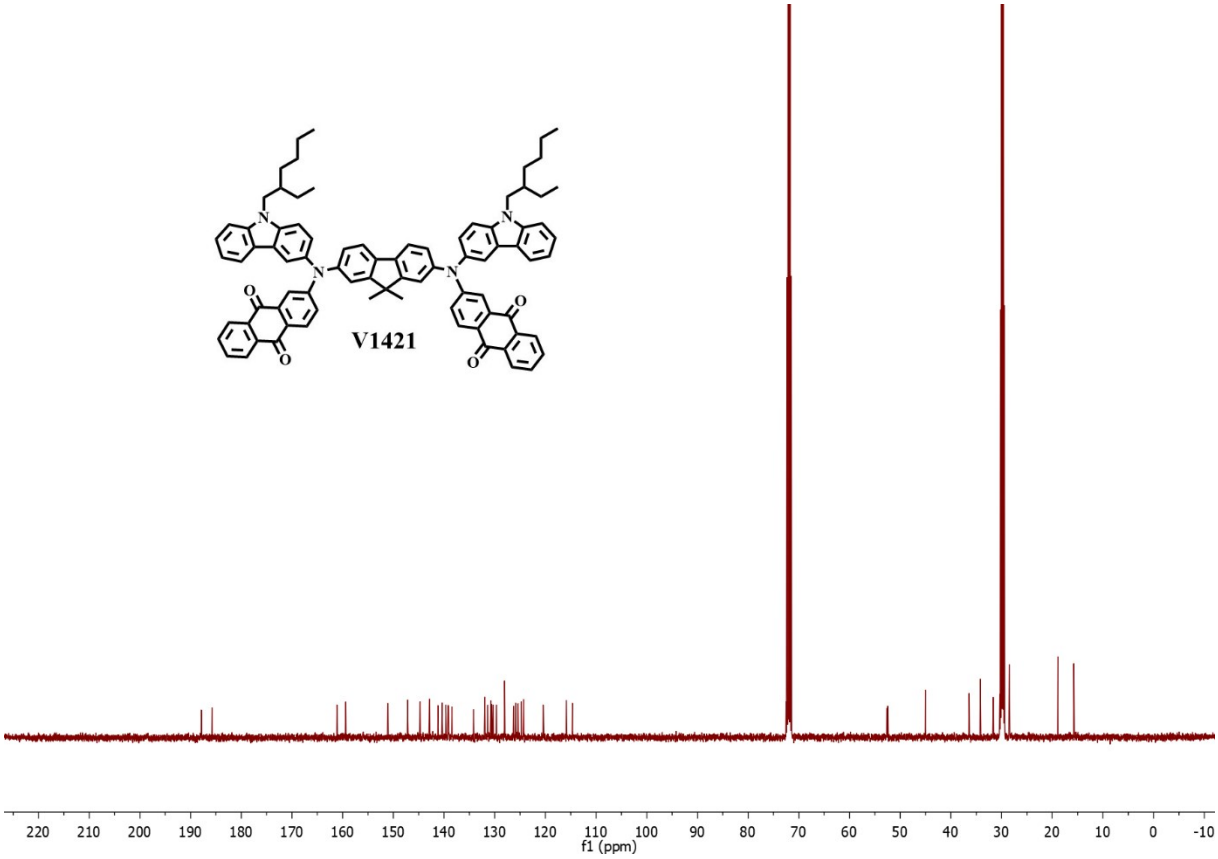

Figure S. 8 ^{13}C NMR spectra of target compound **V1421**.

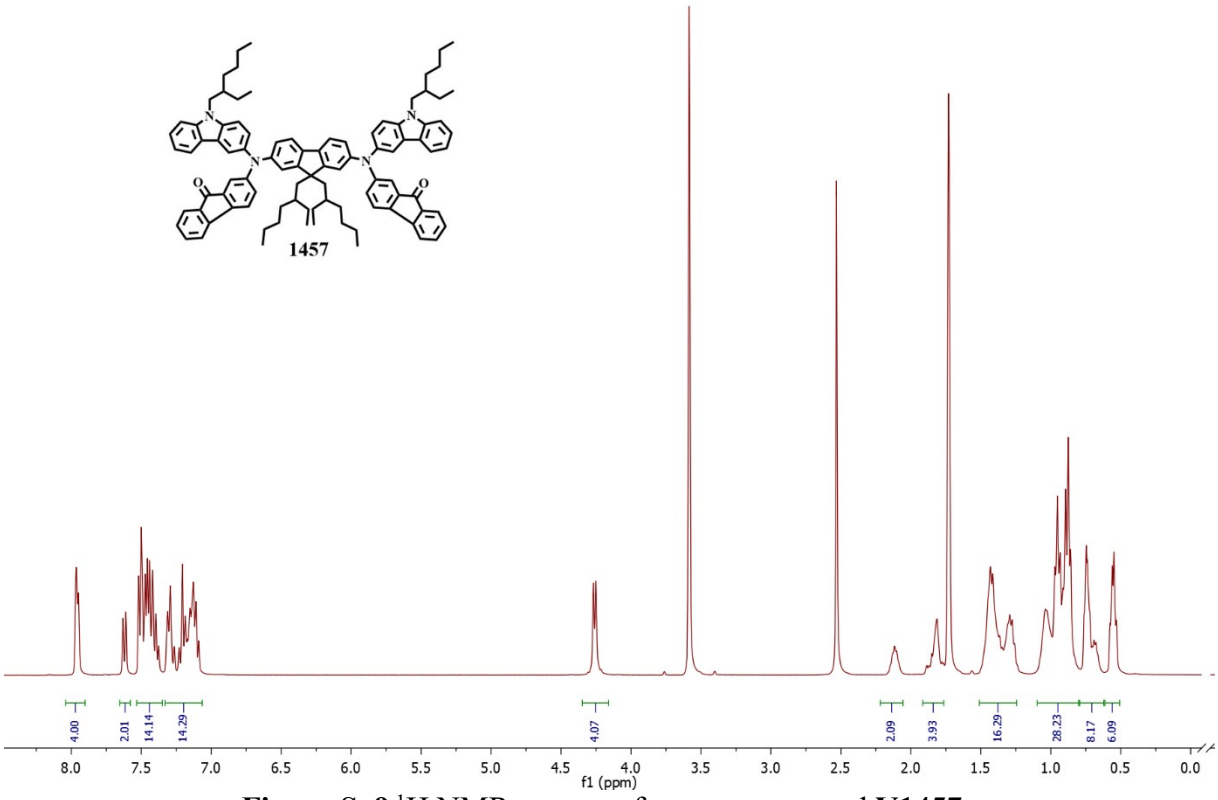

Figure S. 9 ^{1}H NMR spectra of target compound **V1457**.

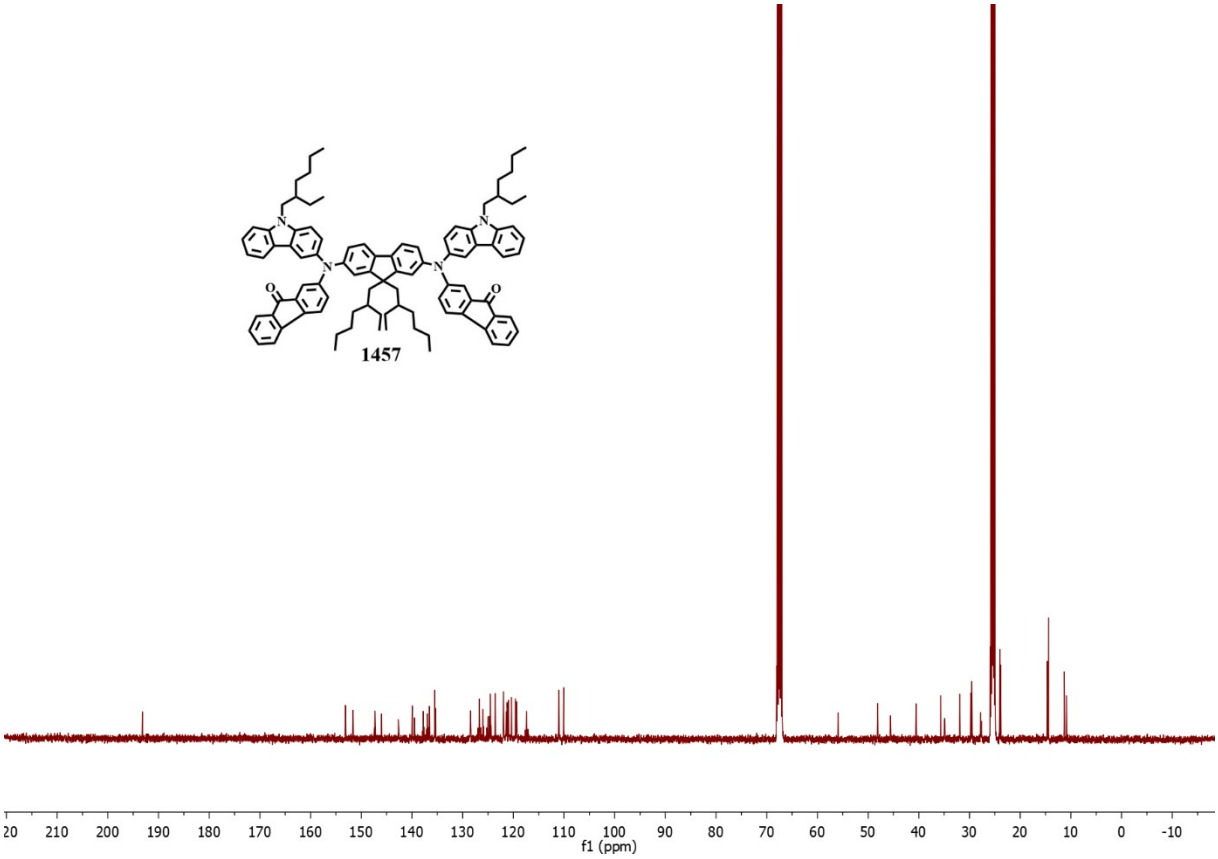

Figure S. 10 ^{13}C NMR spectra of target compound **V1457**.

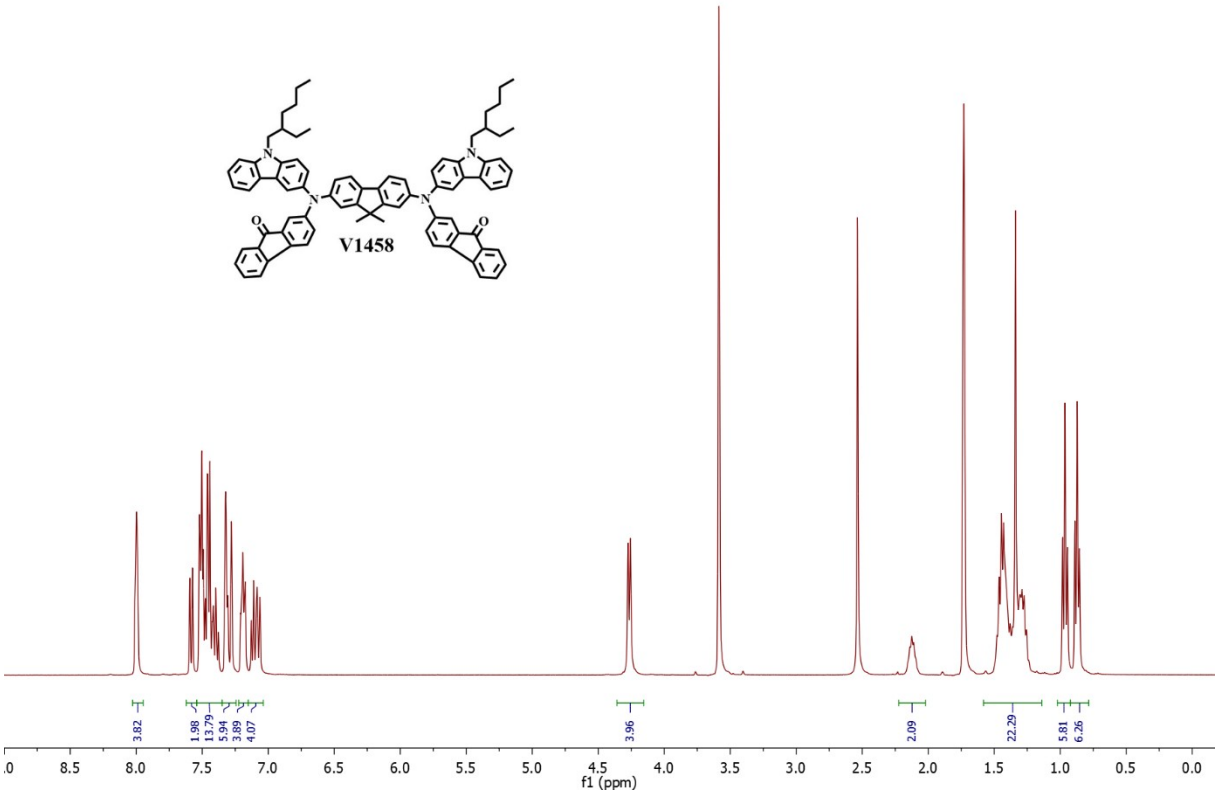

Figure S. 11 ^{1}H NMR spectra of target compound **V1458**.

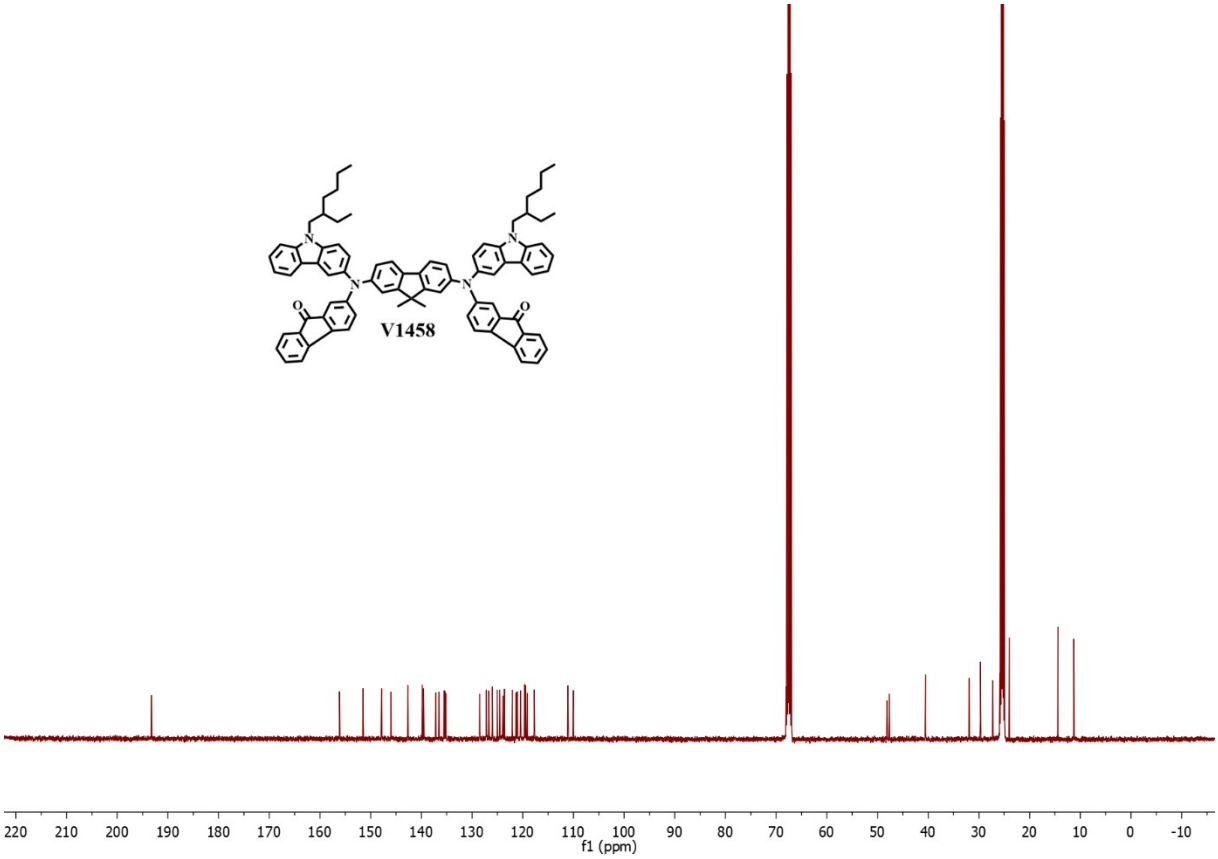

Figure S. 12 ^{13}C NMR spectra of target compound **V1458**.

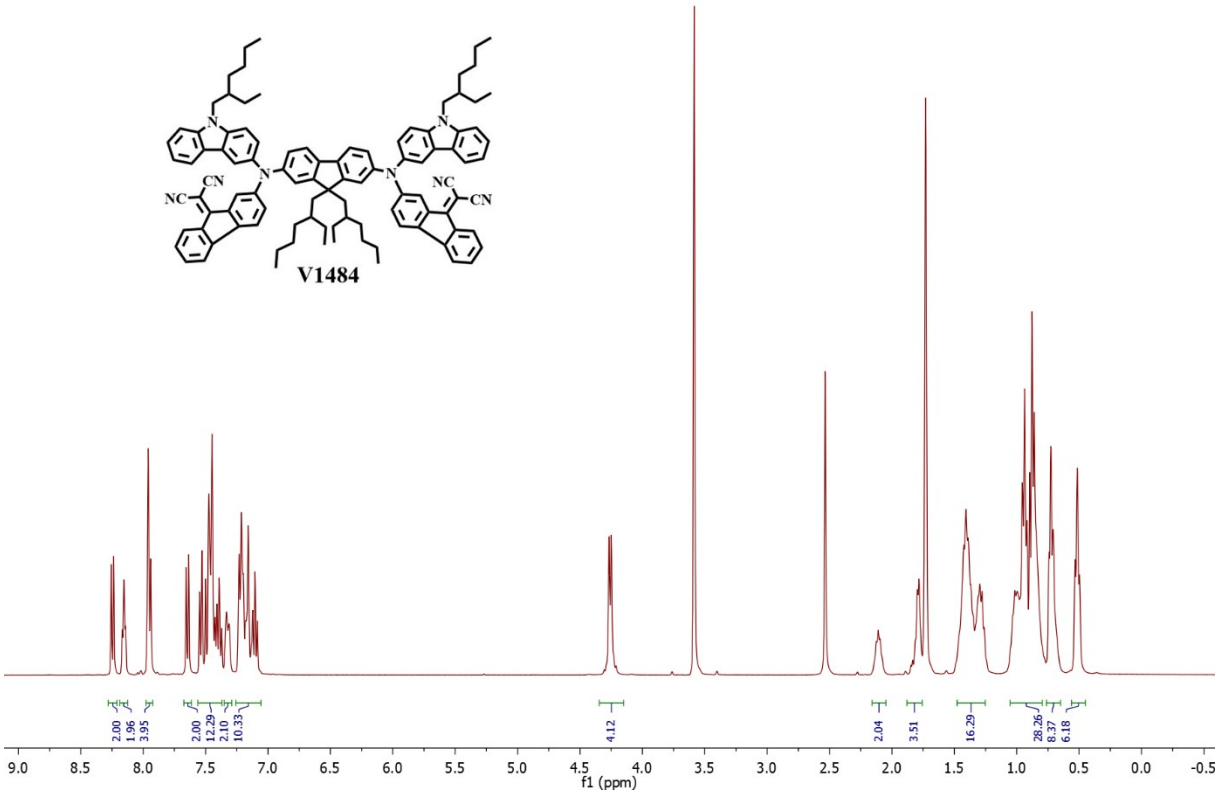

Figure S. 13 ^{1}H NMR spectra of target compound **V1484**.

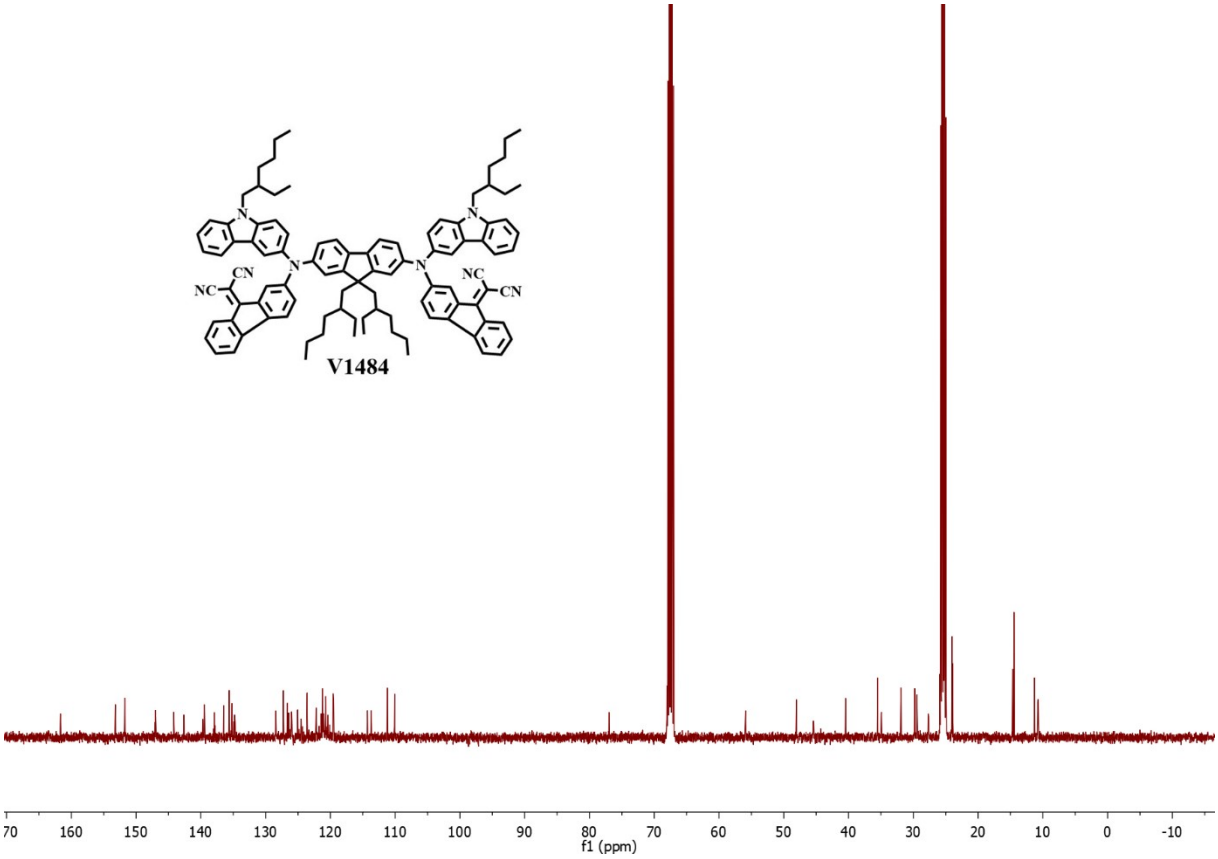

Figure S. 14 ^{13}C NMR spectra of target compound **V1484**.

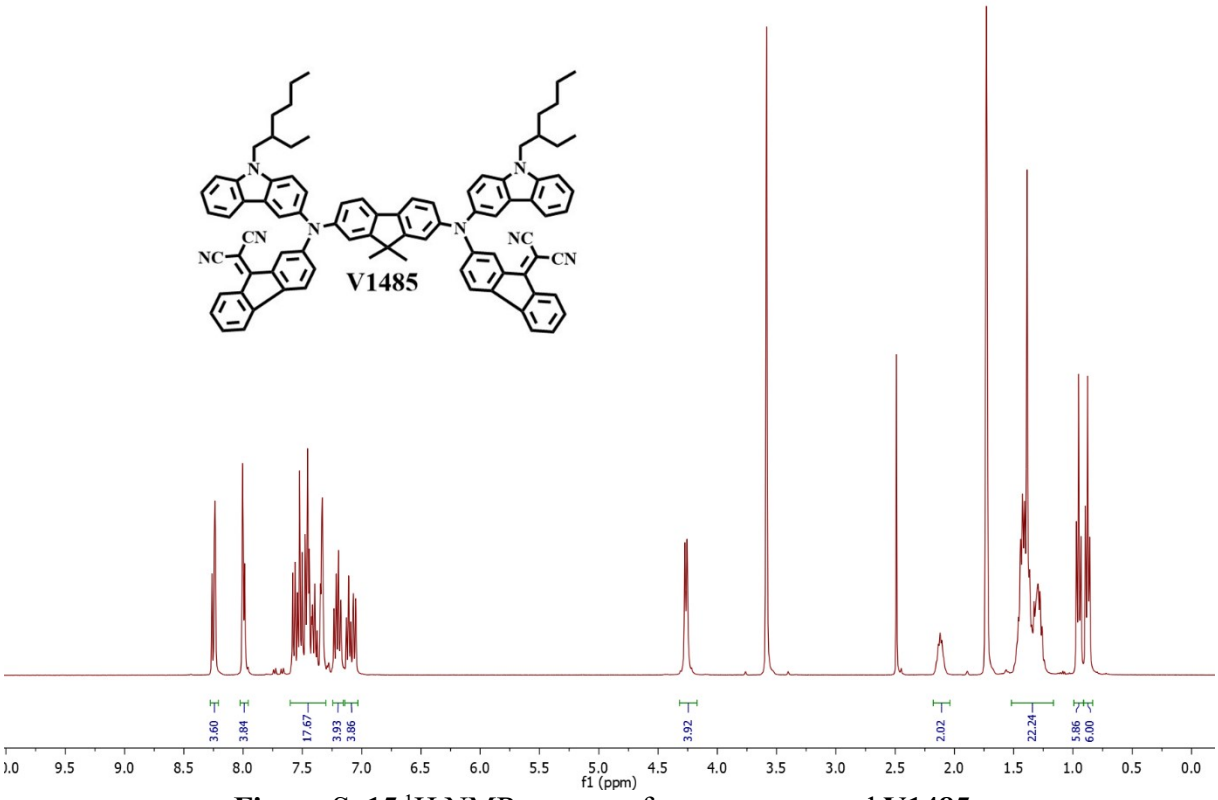

Figure S. 15 ^{1}H NMR spectra of target compound **V1485**.

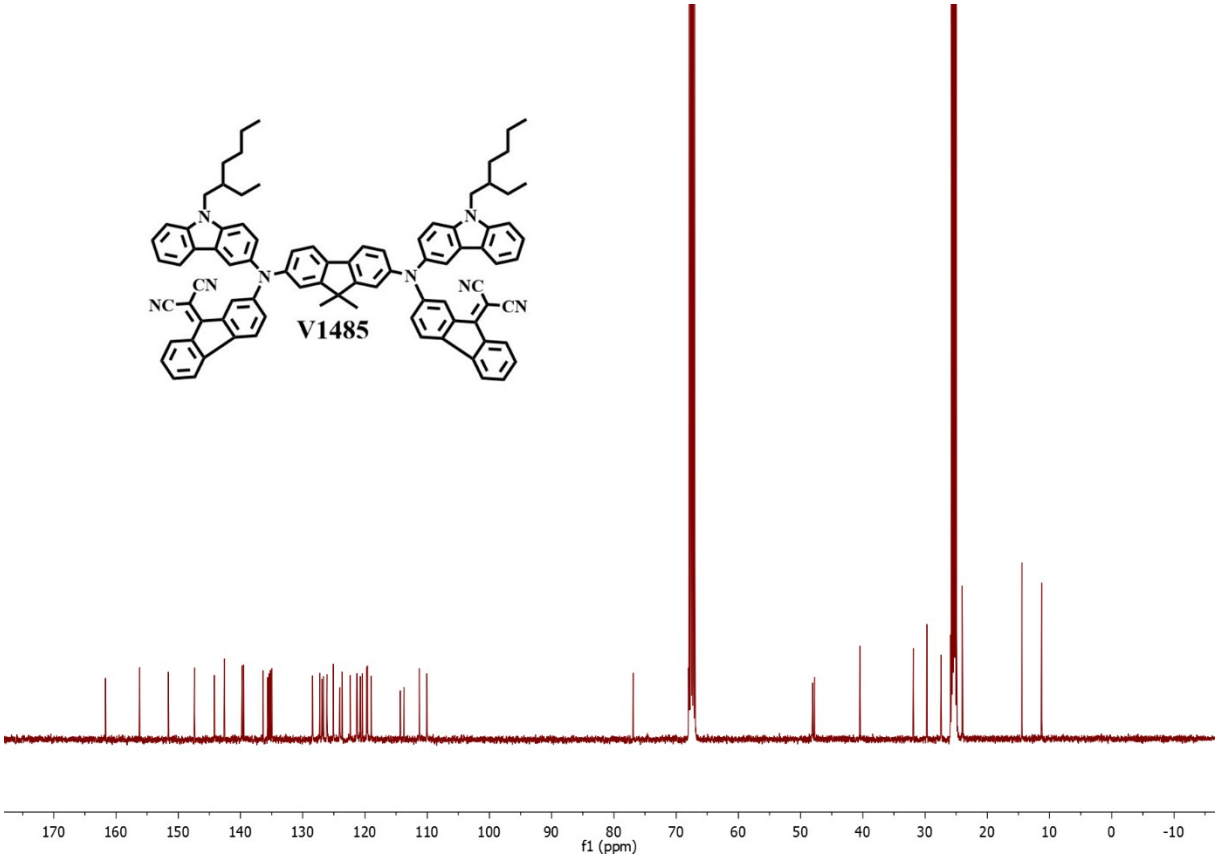

Figure S. 16 ^{13}C NMR spectra of target compound **V1485**.

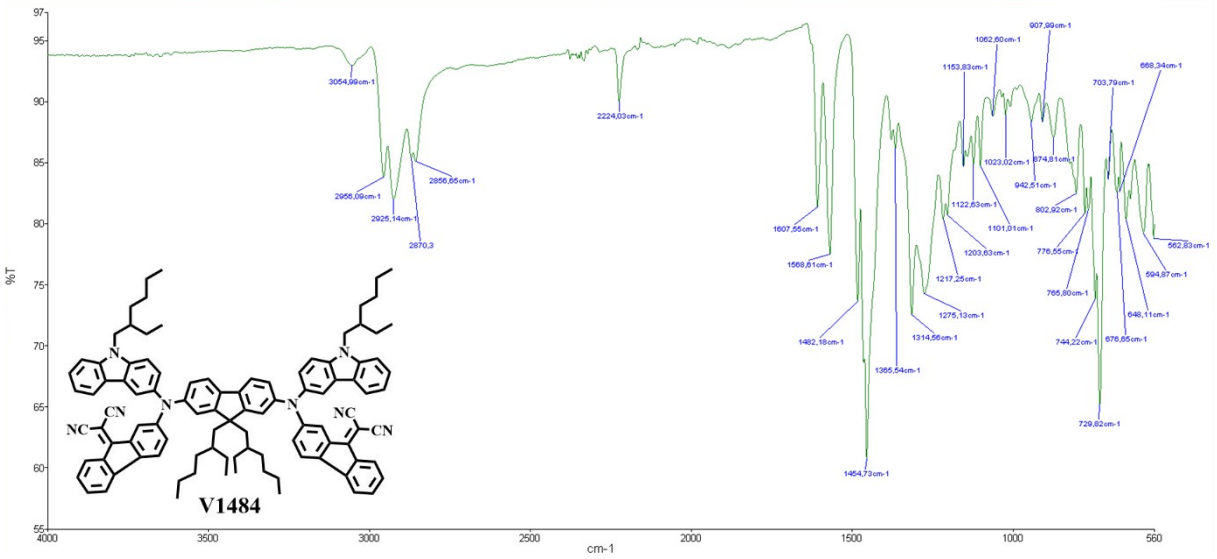

Figure S. 17 IR spectra of target compound **V1484**.

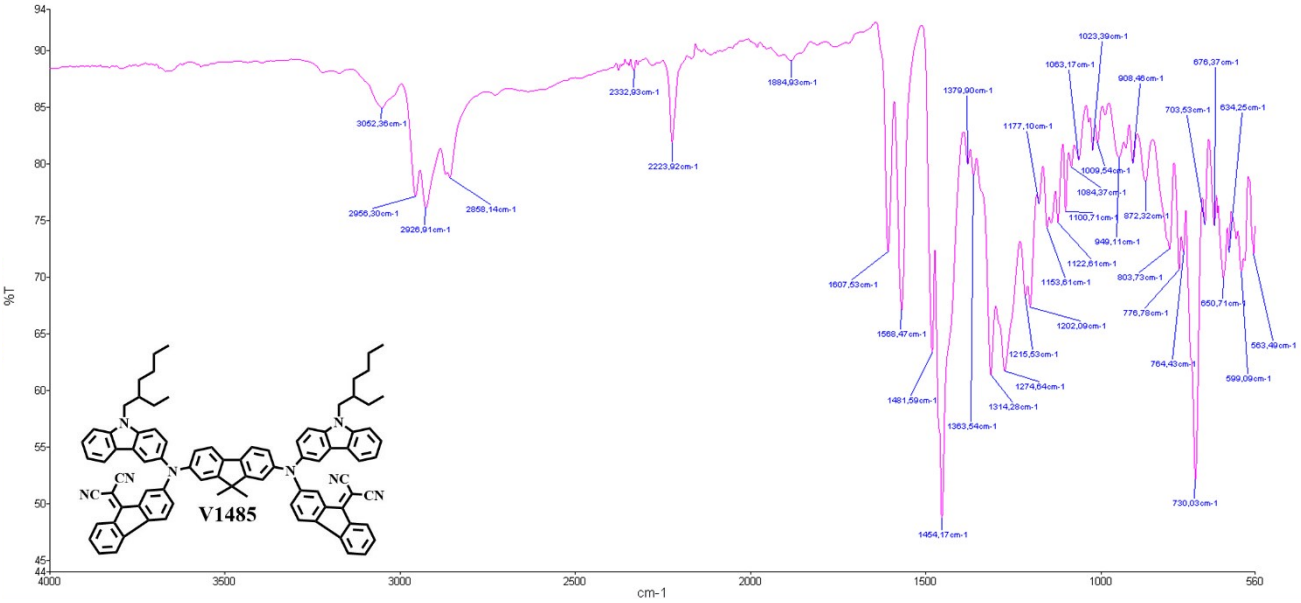

Figure S. 18 IR spectra of target compound **V1485**.

Detailed synthetic procedures

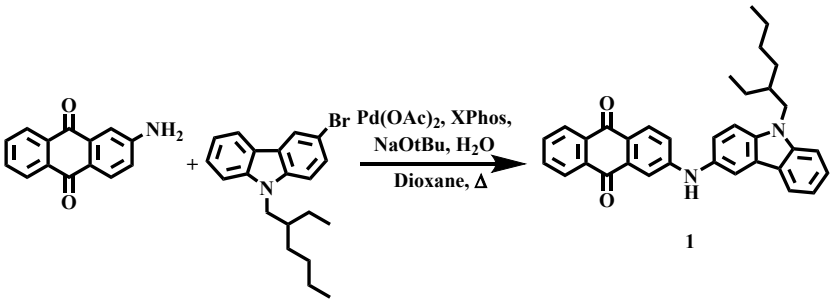

Scheme S1. Synthesis of new amine compound **1**.

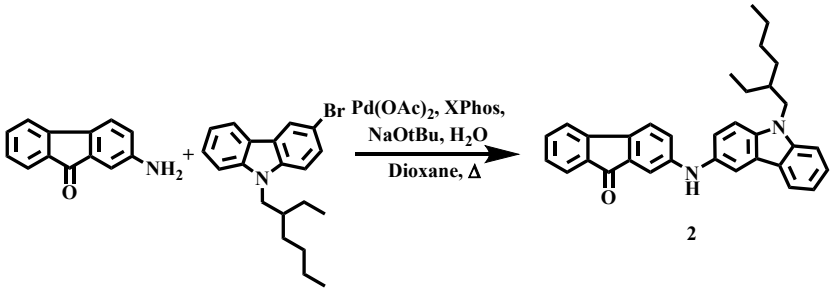

Scheme S2. Synthesis of intermediate product **2**.

2-((9-(2-Ethylhexyl)-9*H*-carbazol-3-yl)amino)anthracene-9,10-dione (1)

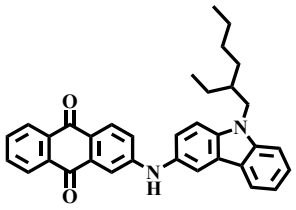

Anhydrous dioxane (15 mL) with a few drops of distilled water (0.5 mmol) added was purged with argon at room temperature for 20 minutes. Then, the temperature was raised to 80 °C, palladium(II) acetate (0.017 g, 0.08 mmol) and XPhos (0.11 g, 0.23 mmol) were added. The mixture was stirred for 1.5 min and temperature was raised to 110 °C. Once the temperature reached 110 °C, 2-aminoanthraquinone (4.1 g, 18 mmol), 3-bromo-9-(2-ethylhexyl)-9*H*-carbazole (5.48 g, 15.3 mmol), and sodium *tert*-butoxide (2.06 g, 21 mmol) were added and the reaction mixture was stirred for 60 minutes (TLC control, THF/*n*-hexane 1:4). Afterwards, the reaction mixture was extracted with ethyl acetate, organic layer was dried over Na_2SO_4, filtered and the solvent was removed by vacuum rotary evaporation. The crude product was purified by column chromatography (THF/*n*-hexane 3:22 v:v), and pearl ruby red residue was collected as a final product. Yield 4.8 g, 63 %.

^{1}H NMR (400 MHz, THF-d_8) δ: 8.36 (s, 1H), 8.24 (d, J = 7.4 Hz, 1H), 8.19 (d, J = 7.5 Hz, 1H), 8.13–7.99 (m, 3H), 7.80–7.65 (m, 3H), 7.56–7.34 (m, 4H), 7.26 (d, J = 8.7 Hz, 1H), 7.15 (t, J = 7.4 Hz, 1H), 4.27 (d, J = 7.4 Hz, 2H), 1.55–1.19 (m, 9H), 0.96 (m, J = 7.4 Hz, 3H), 0.87 (t, J = 7.1 Hz, 3H).

^{13}C NMR (101 MHz, THF-d_8) δ: 183.9, 181.0, 153.3, 142.6, 139.5, 136.4, 135.4, 134.8, 134.6, 133.7, 133.0, 130.4, 127.5, 127.4, 126.7, 124.7, 124.6, 123.5, 122.9, 121.2, 119.6, 118.2, 115.9, 111.0, 110.7, 110.1, 48.1, 40.5, 31.9, 29.7, 24.0, 14.4, 11.3.

FTIR ν (cm^{-1}): 3334 (NH), 3054 ($CH_{arom.}$); 2955, 2926, 2857 ($CH_{alif.}$); 1668 (C=O).

Anal. Calcd. For $C_{34}H_{32}N_2O_2$: C 81.57; H 6.44; N 5.60; O 6.39; found: C 81.61; H 6.42; N 5.57.

$C_{34}H_{32}N_2O_2$ [M^+] exact mass = 500.25, MS (ESI) = 499.01.

2-((9-(2-Ethylhexyl)-9*H*-carbazol-3-yl)amino)-9*H*-fluoren-9-one (2)

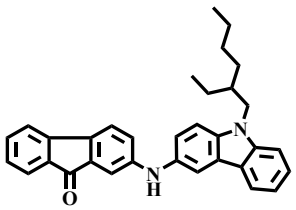

Anhydrous dioxane (17 mL) with a few drops of distilled water (0.5 mmol) added was purged with argon at room temperature for 20 minutes. Then, the temperature was raised to 80 °C, palladium(II) acetate (0.019 g, 0.09 mmol) and XPhos (0.12 g, 0.25 mmol) were added. The mixture was stirred for 1.5 min and temperature was raised to 110 °C. Once the temperature reached 110 °C, 2-amino-9*H*-fluorenone (3.9 g, 20 mmol), 3-bromo-9-(2-ethylhexyl)-9*H*-carbazole (6 g, 17 mmol), and sodium *tert*-butoxide (2.25 g, 23 mmol) were added and the reaction mixture was stirred for 20 minutes (TLC control, THF/*n*-hexane 1:4). Afterwards, the reaction mixture was extracted with ethyl acetate, organic layer was dried over Na_2SO_4, filtered and the solvent was removed by vacuum rotary evaporation. The crude product was purified by column chromatography (acetone/*n*-hexane 3:22 v:v), and purple residue was collected as a final product. Yield 5.14 g, 65 %.

^{1}H NMR (400 MHz, THF-d_8) δ: 8.03 (d, J = 7.8 Hz, 1H), 7.91 (s, 1H), 7.60 (s, 1H), 7.51–7.34 (m, 7H), 7.30 (d, J = 8.6 Hz, 1H), 7.19 (s, 1H), 7.12 (t, J = 7.2 Hz, 2H), 7.04 (d, J = 8.1, 2.3 Hz, 1H), 4.24 (d, J = 7.5 Hz, 2H), 1.55–1.18 (m, 9H), 0.95 (t, J = 7.4 Hz, 3H), 0.87 (t, J = 7.1 Hz, 3H).

^{13}C NMR (101 MHz, THF-d_8) δ: 193.9, 149.5, 146.8, 142.5, 138.7, 136.9, 135.4, 135.2, 134.9, 134.5, 127.7, 126.4, 124.6, 124.4, 123.6, 122.3, 122.2, 121.1, 119.8, 119.3, 119.2, 114.6, 110.8, 110.5, 109.9, 48.0, 40.5, 31.9, 29.7, 24.0, 14.4, 11.3.

FTIR ν (cm^{-1}): 3372 (NH), 3050 ($CH_{arom.}$); 2956, 2927, 2870, 2857 ($CH_{alif.}$); 1705 (C=O).

Anal. Calcd. For $C_{33}H_{32}N_2O$: C 83.86; H 6.82; N 5.93; O 3.39; found: C 83.89; H 6.75; N

5.96.

$C_{33}H_{32}N_2O$ [M^+] exact mass = 472.25, MS (ESI) = 473.57.

2,7-Bis(*N*,*N*-bis[anthracene-9,10-dione-2-yl]-*N*,*N*'-bis[9-(2-ethylhexyl)-9*H*-carbazol-3-yl)amine-9,9-bis(2-ethylhexyl)-9*H*-fluorene (**V1393**)

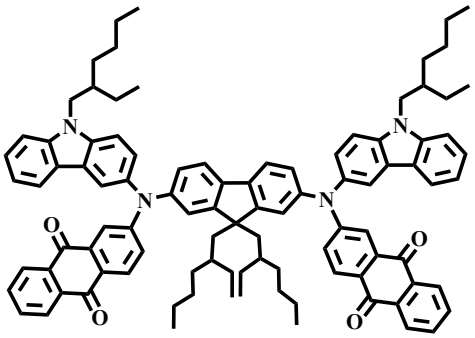

A mixture of 2,7-dibromo-9,9-bis(2-ethylhexyl)-9*H*-fluorene (0.57 g, 1 mmol), 2-((9-(2-ethylhexyl)-9*H*-carbazol-3-yl)amino)anthracene-9,10-dione (**1**) (1.5 g, 3 mmol), and anhydrous toluene (12 mL) was purged with argon for 30 minutes. Afterwards, palladium(II) acetate (0.012 g, 0.05 mmol) and tri-*tert*-butylphosphonium tetrafluoroborate (0.032 g, 0.1 mmol) were added and the reaction mixture was stirred for 10 minutes under argon. Then, sodium *tert*-butoxide (0.29 g, 3 mmol) was added and the mixture was heated at reflux for 6 h (TLC control, toluene/acetone/hexane 5:3:17). After cooling to room temperature, the reaction mixture was filtered through celite and extracted with ethyl acetate. The organic layer was dried over Na_2SO_4, filtered and the solvent was removed by vacuum rotary evaporation. The product was purified by column chromatography (eluent: toluene/acetone/*n*-hexane 5:1:19 v:v:v). The final product was dissolved in THF and precipitated from ethanol to collect the final product as a pearl ruby red powder. Yield 1.22 g, 88 %.

^{1}H NMR (400 MHz, Acetone-d_6) δ: 8.25–8.17 (m, 4H), 8.14 (d, J = 7.5 Hz, 2H), 8.10–8.04 (m, 4H), 7.91–7.77 (m, 6H), 7.69–7.63 (m, 4H), 7.58 (d, J = 8.3 Hz, 2H), 7.54–7.40 (m, 8H), 7.29–7.21 (m, 2H), 7.18 (t, J = 7.4 Hz, 2H), 4.35 (d, J = 7.4 Hz, 4H), 2.19–2.09 (m, 2H), 2.02–

1.83 (m, 4H) 1.49–1.18 (m, 16H), 1.00–0.73 (m, 28H), 0.70–0.54 (m, 8H), 0.46 (q, J = 7.2 Hz, 6H).

^{13}C NMR (101 MHz, Acetone-d_6) δ: 183.7, 181.5, 155.2, 153.8, 145.8, 142.5, 140.2, 139.4, 138.0, 135.8, 135.02, 134.95, 134.5, 134.3, 129.7, 127.5, 127.4, 127.1, 126.8, 126.5, 125.34, 125.27, 124.9, 123.7, 123.3, 122.4, 121.9, 121.4, 120.4, 119.9, 114.8, 111.7, 110.5, 56.2, 48.0, 45.2, 40.3, 35.6, 34.8, 31.6, 27.4, 27.3, 25.1, 23.8, 23.5, 14.4, 14.3, 11.3, 10.62, 10.60.

FTIR ν (cm^{-1}): 3050 ($CH_{arom.}$); 2956, 2925, 2857 ($CH_{alif.}$); 1672 (C=O).

Anal. Calcd. For $C_{97}H_{102}N_4O_4$: C 83.94; H 7.41; N 4.04; O 4.61; found: C 83.89; H 7.45; N 4.07.

$C_{97}H_{102}N_4O_4$ [M^+] exact mass = 1386.79, MS (ESI) = 1387.68.

2,7-Bis(*N*,*N*-bis[anthracene-9,10-dione-2-yl]-*N*,*N*'-bis[9-(2-ethylhexyl)-9*H*-carbazol-3-yl)amine-9,9-dimethyl-9*H*-fluorene (**V1421**)

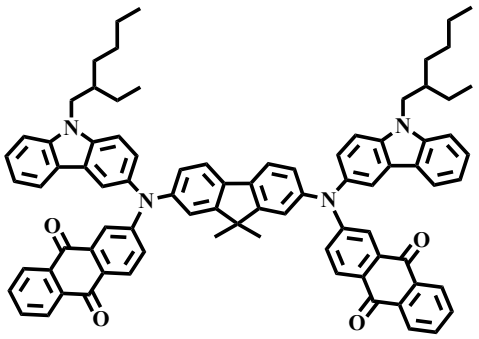

A mixture of 2,7-dibromo-9,9-dimethyl-9*H*-fluorene (0.55 g, 1.6 mmol), 2-((9-(2-ethylhexyl)-9*H*-carbazol-3-yl)amino)anthracene-9,10-dione (**1**) (2.4 g, 4.8 mmol), and anhydrous toluene (15 mL) was purged with argon for 30 minutes. Afterwards, palladium(II) acetate (0.02 g, 0.09 mmol) and tri-*tert*-butylphosphonium tetrafluoroborate (0.052 g, 0.18 mmol) were added and the reaction mixture was stirred for 10 minutes under argon. Then, sodium *tert*-butoxide (0.46 g, 4.8 mmol) was added and the mixture was heated at reflux for 5 h (TLC control, toluene/acetone/hexane 5:3:17). After cooling to room temperature, the

reaction mixture was filtered through celite and extracted with ethyl acetate. The organic layer was dried over Na_2SO_4, filtered and the solvent was removed by vacuum rotary evaporation. The product was purified by column chromatography (eluent: toluene/acetone/*n*-hexane 6:1:18 v:v:v). The final product was dissolved in THF and precipitated from methanol to collect the final product as a pearl ruby red powder. Yield 1.58 g, 83 %.

^{1}H NMR (400 MHz, THF-d_8) δ: 8.24 (d, J = 7.5 Hz, 2H), 8.16 (d, J = 7.5 Hz, 2H), 8.13–8.00 (m, 6H), 7.84–7.69 (m, 8H), 7.58 (d, J = 8.6 Hz, 2H), 7.53–7.47 (m, 4H), 7.46–7.37 (m, 4H), 7.31 (dd, J = 8.8, 2.6 Hz, 2H), 7.24 (d, J = 8.1 Hz, 2H), 7.15 (t, J = 7.5 Hz, 2H), 4.30 (d, J = 7.4 Hz, 4H), 2.20 – 2.05 (m, 2H), 1.55–1.22 (m, 22H), 0.97 (t, J = 7.4 Hz, 6H), 0.88 (t, J = 7.1 Hz, 6H).

^{13}C NMR (101 MHz, THF) δ: 187.9, 185.8, 161.1, 159.4, 151.1, 147.2, 144.7, 142.9, 141.2, 140.4, 139.7, 139.2, 139.1, 138.4, 134.2, 132.0, 131.4, 130.8, 130.6, 130.3, 129.7, 128.1, 126.3, 125.9, 125.4, 124.7, 124.3, 120.4, 115.9, 114.7, 52.6, 52.4, 45.0, 36.4, 34.2, 31.6, 28.5, 18.9, 15.8.

FTIR ν (cm^{-1}): 3321, 3064 ($CH_{arom.}$); 2959, 2927, 2858,($CH_{alif.}$); 1671 (C=O).

Anal. Calcd. For $C_{83}H_{74}N_4O_4$: C 83.67; H 6.26; N 4.70; O 5.37; found: C 83.71; H 6.23; N 4.72.

$C_{83}H_{74}N_4O_4$ [M^+] exact mass = 1190.57, MS (ESI) = 1191.56.

2,7-*N*,*N*'-bis[9-(2-ethylhexyl)-9*H*-carbazol-3-yl)]-*N*,*N*-bis[9*H*-fluoren-9-one]amine-9,9-bis(2-ethylhexyl)-9*H*-fluorene (V1457)

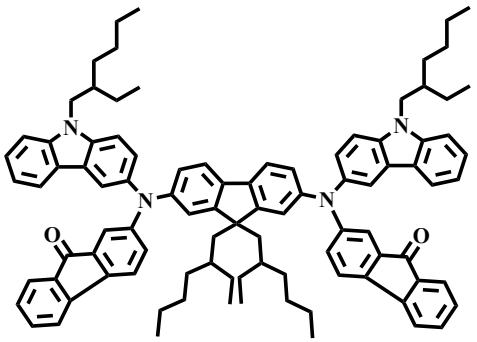

A mixture of 2,7-dibromo-9,9-bis(2-ethylhexyl)-9*H*-fluorene (0.45 g, 0.8 mmol), 2-((9-(2-ethylhexyl)-9*H*-carbazol-3-yl)amino)-9*H*-fluoren-9-one (**2**) (1.1 g, 2.4 mmol), and anhydrous toluene (8 mL) was purged with argon for 30 minutes. Afterwards, palladium(II) acetate (0.01 g, 0.04 mmol) and tri-*tert*-butylphosphonium tetrafluoroborate (0.026 g, 0.09 mmol) were added and the reaction mixture was stirred for 10 minutes under argon. Then, sodium *tert*-butoxide (0.23 g, 2.4 mmol) was added and the mixture was heated at reflux for 15 h (TLC control, acetone/hexane 1:24). After cooling to room temperature, the reaction mixture was filtered through celite and extracted with ethyl acetate. The organic layer was dried over Na_2SO_4, filtered and the solvent was removed by vacuum rotary evaporation. The product was purified by column chromatography (eluent: acetone/*n*-hexane 1:24 v:v). The final product was dissolved in THF and precipitated from ethanol to collect the final product as a cherish red powder. Yield 0.8 g, 75 %.

^{1}H NMR (400 MHz, THF-d_8) δ: 8.02–7.89 (m, 4H), 7.62 (d, J = 8.2 Hz, 2H), 7.55–7.35 (m, 14H), 7.33–7.06 (m, 14H), 4.26 (d, J = 7.4 Hz, 4H), 2.23–2.06 (m, 2H), 1.92–1.77 (m, 4H), 1.51–1.21 (m, 16H), 1.11 – 0.82 (m, 28H), 0.80 – 0.62 (m, 8H), 0.62 – 0.49 (m, 6H).

^{13}C NMR (101 MHz, THF) δ: 193.2, 153.1, 151.6, 147.4, 147.3, 146.0, 142.7, 139.9, 139.5, 137.8, 137.0, 136.6, 135.5, 135.4, 128.4, 126.7, 126.0, 125.0, 124.7, 124.5, 123.6, 122.0, 121.4, 121.2, 121.0, 120.4, 119.6, 119.4, 117.4, 111.0, 110.1, 55.9, 48.1, 45.6, 40.6, 35.70, 35.67, 34.9, 31.9, 29.8, 29.6, 27.8, 27.7, 24.0, 23.9, 14.6, 14.4, 11.3, 10.9, 10.8.

FTIR ν (cm^{-1}): 3414, 3051 ($CH_{arom.}$); 2956, 2925, 2857 ($CH_{alif.}$); 1714 (C=O).

Anal. Calcd. For $C_{95}H_{102}N_4O_2$: C 85.67; H 7.72; N 4.21; O 2.40; found: C 85.70; H 7.69; N 4.23.

$C_{95}H_{102}N_4O_4$ [M^+] exact mass = 1330.80, MS (ESI) = 1331.88.

2,7-*N,N'*-bis[9-(2-ethylhexyl)-9*H*-carbazol-3-yl)]-*N,N*-bis[9*H*-fluoren-9-one]amine-9,9-dimethyl-9*H*-fluorene (**V1458**)

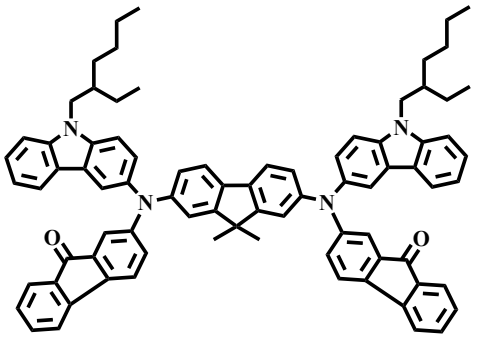

A mixture of 2,7-dibromo-9,9-dimethyl-9*H*-fluorene (0.35 g, 1 mmol), 2-((9-(2-ethylhexyl)-9*H*-carbazol-3-yl)amino)-9*H*-fluoren-9-one (**2**) (1.4 g, 3 mmol), and anhydrous toluene (9 mL) was purged with argon for 30 minutes. Afterwards, palladium(II) acetate (0.013 g, 0.06 mmol) and tri-*tert*-butylphosphonium tetrafluoroborate (0.032 g, 0.1 mmol) were added and the reaction mixture was stirred for 10 minutes under argon. Then, sodium *tert*-butoxide (0.29 g, 3 mmol) was added and the mixture was heated at reflux for 8 h (TLC control, toluene/acetone/hexane 5:3:17). After cooling to room temperature, the reaction mixture was filtered through celite and extracted with ethyl acetate. The organic layer was dried over Na_2SO_4, filtered and the solvent was removed by vacuum rotary evaporation. The product was purified by column chromatography (eluent: toluene/acetone/*n*-hexane 4:1:20 v:v:v). The final product was dissolved in THF and precipitated from methanol to collect the final product as a cherish red powder. Yield 0.75 g, 66 %.

^{1}H NMR (400 MHz, THF-d_8) δ: 8.03–7.95 (m, 4H), 7.58 (d, J = 8.2 Hz, 2H), 7.54–7.36 (m, 14H), 7.36–7.24 (m, 6H), 7.24–7.14 (m, 4H), 7.14–7.03 (m, 4H), 4.26 (d, J = 7.4 Hz, 4H), 2.21–2.03 (m, 2H), 1.58–1.13 (m, 22H), 0.96 (t, J = 7.4 Hz, 6H), 0.87 (t, J = 7.0 Hz, 6H).

^{13}C NMR (101 MHz, THF) δ: 193.2, 156.2, 151.5, 147.8, 146.0, 142.6, 139.8, 139.6, 137.2, 136.5, 135.5, 135.4, 135.2, 128.5, 127.2, 126.7, 126.0, 125.0, 124.5, 123.9, 123.6, 122.1, 121.3, 121.1, 120.4, 119.6, 119.5, 119.1, 117.7, 111.1, 110.0, 48.1, 47.7, 40.6, 31.9, 29.7, 27.7, 24.0, 14.4, 11.3.

FTIR ν (cm^{-1}): 3050 ($CH_{arom.}$); 2956, 2926, 2858 ($CH_{alif.}$); 1714 (C=O).

Anal. Calcd. For $C_{81}H_{74}N_4O_2$: C 85.68; H 6.57; N 4.93; O 2.82; found: C 85.72; H 6.54; N 4.90.

$C_{81}H_{74}N_4O_2$ [M^+] exact mass = 1134.58, MS (ESI) = 1135.30.

2,7-*N,N'*-bis[9-(2-ethylhexyl)-9*H*-carbazol-3-yl)]-*N,N*-bis[diciano-9-ylidene-9*H*-fluorene-2-yl]amine-9,9-bis(2-ethylhexyl)-9*H*-fluorene (**V1484**)

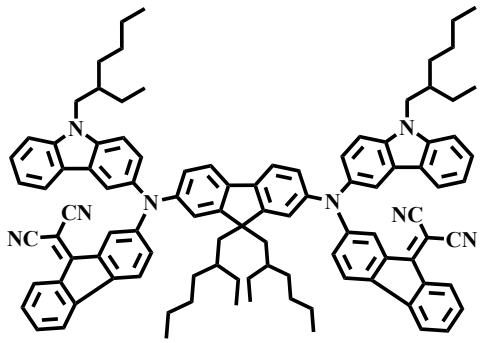

A mixture of 2,2'-((9,9-bis(2-ethylhexyl)-9*H*-fluorene-2,7-diyl)bis((9-(2-ethylhexyl)-9*H*-carbazol-3-yl)azanediyl))bis(9*H*-fluoren-9-one) (**V1457**) (0.65 g, 0.5 mmol), malononitrile (0.07 g, 1.1 mmol), and THF (6.5 mL) was stirred for a few minutes. Afterwards, triethylamine (0.45 mL, 3 mmol) was added slowly drop-by-drop, and the reaction mixture was stirred at 35^{o}C for 16 h (TLC control, acetone/hexane 1:4). After cooling to room temperature, the reaction mixture was extracted with ethyl acetate. The organic layer was dried over Na_2SO_4, filtered and the solvent was removed by vacuum rotary evaporation. The product was purified

by column chromatography (eluent: acetone/*n*-hexane 2:23 v:v). The final product was dissolved in acetone and precipitated from ethanol to collect the final product as a moss green powder. Yield 0.5 g, 70 %.

^{1}H NMR (400 MHz, THF-d_8) δ: 8.25 (d, J = 7.8 Hz, 2H), 8.15 (t, J = 5.5 Hz, 2H), 7.97–7.92 (m, 4H), 7.65 (d, J = 8.2 Hz, 2H), 7.56–7.36 (m, 12H), 7.35–7.29 (m, 2H), 7.26–7.06 (m, 10H), 4.26 (d, J = 7.5 Hz, 4H), 2.16–2.05 (m, 2H), 1.88–1.76 (m, 4H), 1.51–1.31 (m, 16H), 1.09–0.79 (m, 28H) 0.76–0.62 (m, 8H), 0.51 (t, J = 7.4 Hz, 6H).

^{13}C NMR (101 MHz, THF) δ: 161.7, 153.2, 151.8, 147.0, 142.6, 139.7, 139.4, 136.5, 135.6, 135.2, 128.4, 127.3, 126.6, 126.4, 126.0, 125.1, 124.5, 123.6, 122.2, 121.4, 121.2, 121.1, 120.8, 120.4, 119.6, 119.5, 114.3, 113.7, 111.2, 110.1, 77.0, 55.9, 48.1, 45.4, 40.5, 35.5, 34.9, 31.9, 29.8, 29.4, 27.7, 27.6, 24.0, 23.9, 14.8, 14.7, 14.5, 11.3, 10.7.

FTIR ν (cm^{-1}): 3054 ($CH_{arom.}$); 2956, 2925, 2870, 2857 ($CH_{alif.}$); 2224 (CN).

Anal. Calcd. For $C_{101}H_{102}N_8$: C 84.95; H 7.20; N 7.85; found: C 84.93; H 7.22; N 7.85.

$C_{101}H_{102}N_8$ [M^+] exact mass = 1426.82, MS (ESI) = 1427.269

2,7-*N,N'*-bis[9-(2-ethylhexyl)-9*H*-carbazol-3-yl)]-*N,N*-bis[diciano-9-ylidene-9*H*-fluorene-2-yl]amine-9,9-dimethyl-9*H*-fluorene (V1485)

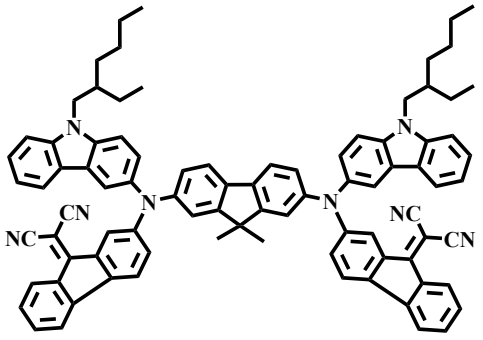

A mixture of 2,2'-((9,9-dimethyl-9*H*-fluorene-2,7-diyl)bis((9-(2-ethylhexyl)-9*H*-carbazol-3-yl)azanediyl))bis(9*H*-fluoren-9-one) (**V1458**) (0.74 g, 0.7 mmol), malononitrile (0.1 g, 1.5 mmol), and THF (7 mL) was stirred for a few minutes. Afterwards, triethylamine (0.6 mL, 4.2

mmol) was slowly added drop-by-drop and the reaction mixture was stirred at 35°C for 16 h (TLC control, acetone/hexane 1:4). After cooling to room temperature, the reaction mixture was extracted with ethyl acetate. The organic layer was dried over Na_2SO_4, filtered and the solvent was removed by vacuum rotary evaporation. The product was purified by column chromatography (eluent: acetone/*n*-hexane 1:4 v:v). The final product was dissolved in THF and precipitated from methanol to collect the final product as a moss green powder. Yield 0.49 g, 57 %.

^{1}H NMR (400 MHz, THF-d_8) δ: 8.28–8.20 (m, 4H), 8.02–7.95 (m, 4H), 7.60–7.30 (m, 18H), 7.25–7.16 (m, 4H), 7.14–7.03 (m, 4H), 4.26 (d, J = 7.4 Hz, 4H), 2.18 – 2.04 (m, 2H), 1.51–1.17 (m, 22H), 0.95 (t, J = 7.4 Hz, 6H), 0.88 (t, J = 7.1 Hz, 6H).

^{13}C NMR (101 MHz, THF) δ: 161.7, 156.2, 151.6, 147.4, 144.2, 142.6, 139.8, 139.5, 136.4, 135.6, 135.4, 135.2, 135.0, 128.4, 127.3, 126.9, 126.7, 126.1, 125.1, 124.1, 123.6, 122.4, 121.3, 121.3, 120.8, 120.4, 119.7, 119.6, 119.0, 114.3, 113.7, 111.3, 110.1, 76.9, 48.1, 47.8, 40.5, 31.9, 29.7, 27.4, 24.0, 14.4, 11.3.

FTIR ν (cm^{-1}): 3052 ($CH_{arom.}$); 2956, 2926, 2858 ($CH_{alif.}$); 2224 (CN).

Anal. Calcd. For $C_{87}H_{74}N_8$: C 84.85; H 6.06; N 9.10; found: C 84.90; H 6.01; N 9.09.

$C_{87}H_{74}N_8$ [M^+] exact mass = 1230.60, MS (ESI) = 1231.40.

Ionization Potential and Cyclic Voltammetry Measurements

The ionization potential was measured by the electron photoemission method in air. The sample solutions (THF) were poured onto an aluminum-coated polyester film coated with an adhesive layer of a copolymer of methyl methacrylate and methacrylic acid. A diffraction grating monochromator with a deuterium lamp was used for the experiment. The power of the falling light was ~ $5 \cdot 10^{-8}$ W. A negative voltage (-100 V) was connected to the test sample. The electron photoemission current was measured with an open Geiger–Müller counter [2]. The

measurement method error was evaluated as 0.03 eV.

Electrochemical studies were carried out by three-electrode assembly cell and potentiostat-galvanostat Bio-Logic SP-150. Measurements were carried out with a glassy carbon electrode in acetonitrile solutions containing 0.1 M tetrabutylammonium hexafluorophosphate as electrolyte, Pt wire was used as the reference electrode, and Pt wire was a counter electrode at a scan rate 50 mV s^{-1}. Each measurement was calibrated with ferrocene (Fc) and potentials were calculated *vs* Fc^{+}/Fc. The half wave potentials $E_{1/2\ vs\ Fc}$ were obtained as an average value between oxidation and reduction peaks. $E_{ox\ vs\ vacuum}$ value was calculated using conversion factors as follows: ferrocene in acetonitrile *vs* SCE (Saturated Calomel Electrode): 0.40;[3] SCE *vs* SHE (Standard Hydrogen Electrode): 0.244;[4] SHE *vs* vacuum: 4.430.[5] E_{LUMO} was calculated from the equation $E_{LUMO} = (E\ vs\ Fc/Fc^{+} + 0.4 + 0.244 + 4.43$.

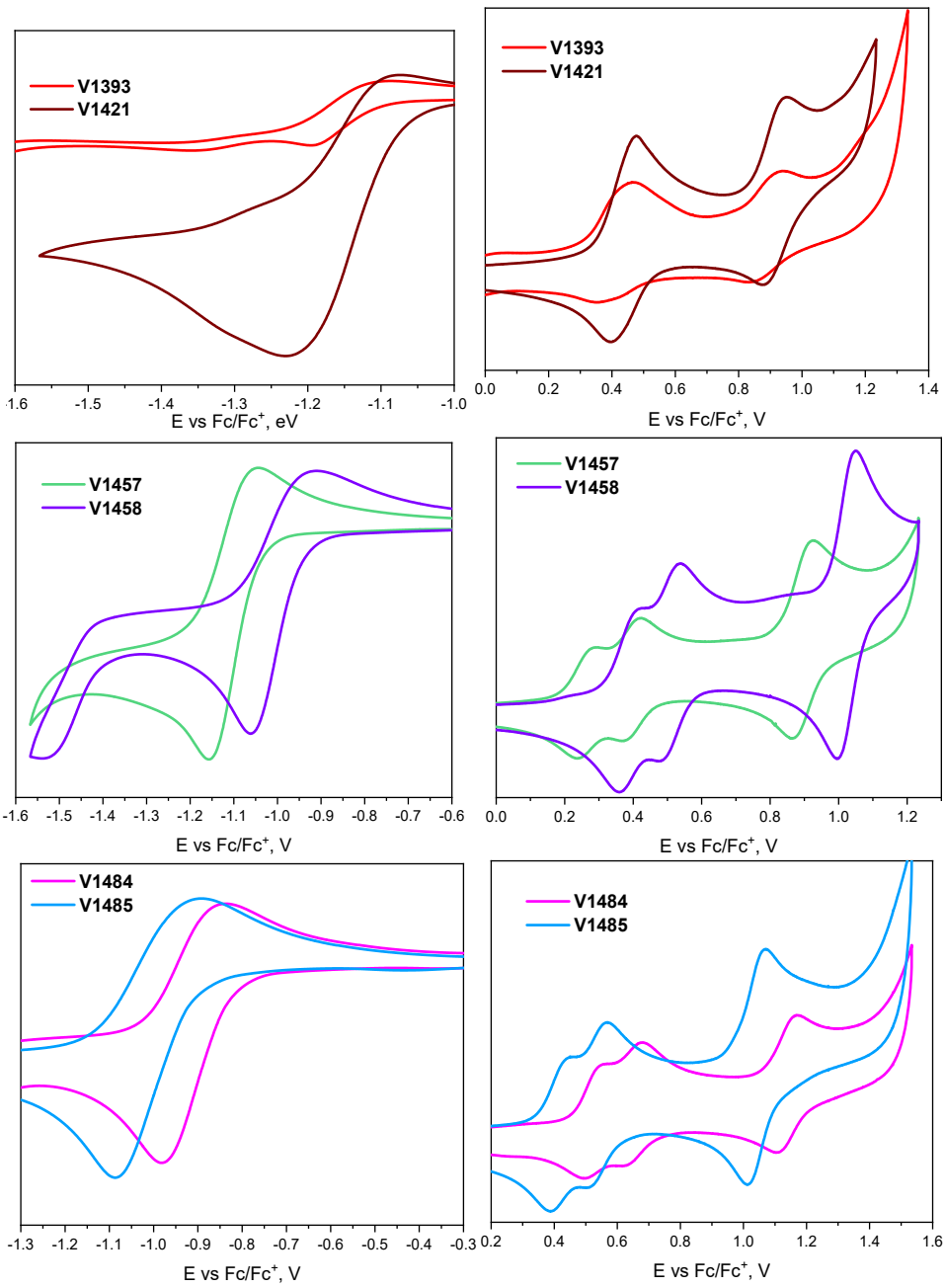

Figure S19. Cyclic voltammetry curves of new compounds **V1393**, **V1421**, **V1457**, **V1458**, **V1484**, and **V1485**.

Quantum chemistry study

Simulations of ground state molecular structure for several most probable conformers were carried out using *Gaussian16* software by means of density functional (DFT) CAM-B3LYP method and 6-31G(d,p) basis set supplemented with polarization functions (d,p). List of several most probable molecular conformations is presented in **Table S1**. One most informative projection (xy) of the mentioned conformations is presented in **Figures S2–S4**. Those

structures were obtained using grad optimization technique (convergence of parameters Maximum Force, RMS Force, Maximum Displacement, RMS Displacement has been achieved). Electronic excitations were simulated using semiempirical TD method (for singlets). The parameters of electronic excitations (transition energy $\Delta E_1(S_0 \rightarrow S_1)$, $\Delta E_2(S_0 \rightarrow S_2)$ and corresponding oscillator strengths f_1, f_2) are presented in **Table S2** for all structures (three conformers for **V1421**, **V1458**, and **V1485** and four conformers for **V1393**, **V1457**, and **V1484**).

Table S1. List of molecular conformations of the compounds.

Compound	Two most probable conformers	Molecular structure after ground state energy optimization using *Gaussian16*, CAM-B3LYP/6-31G(d,p) basis set
V1421	V1421a, V1421b	Fig. S20
V1393	V1393a, V1393b	Fig. S20
V1458	V1458a, V1458b	Fig. S21
V1457	V1457a, V1457b	Fig. S21
V1485	V1485a, V1485b	Fig. S22
V1484	V1484a, V1484b	Fig. S22

xy	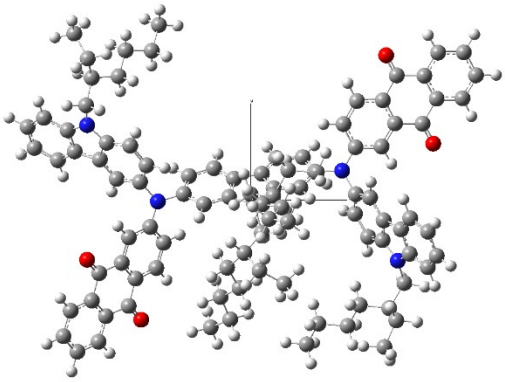	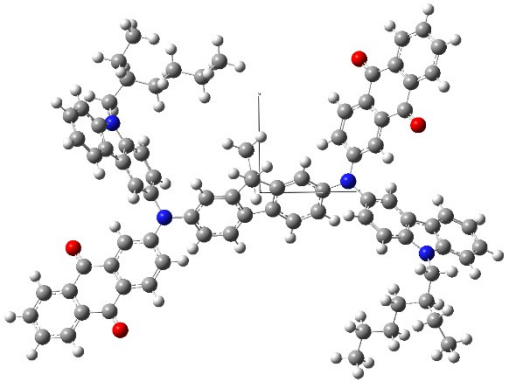
Conformer	V1393a	V1421a
xy	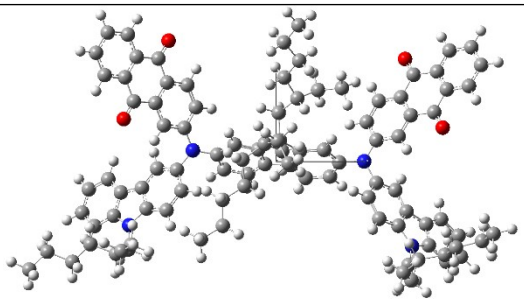	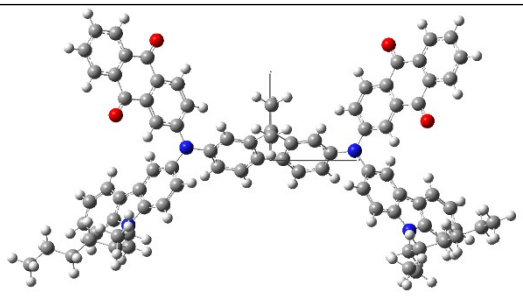
Conformer	V1393b	V1421b

Fig. S20. V1393 and **V1421** compounds. Molecular structure of two conformers in xy projection after ground state energy optimization routine using *Gaussian16*, CAM-B3LYP/6-31G(d,p) basis set.

xy	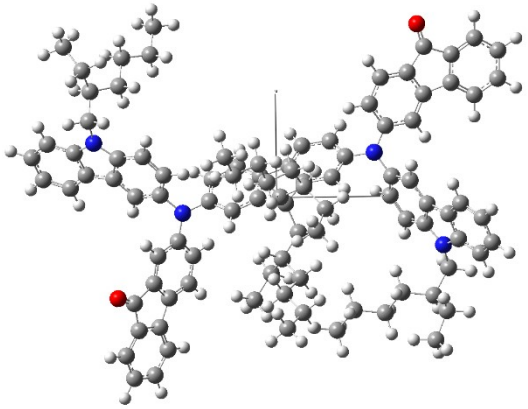	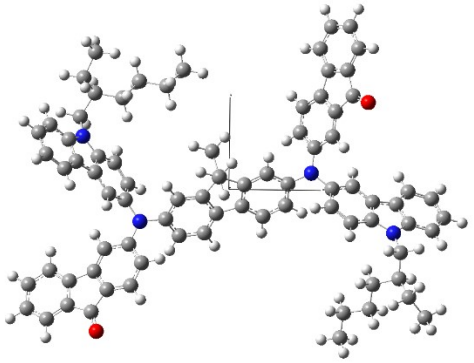
Conformer	V1457a	V1458a
xy	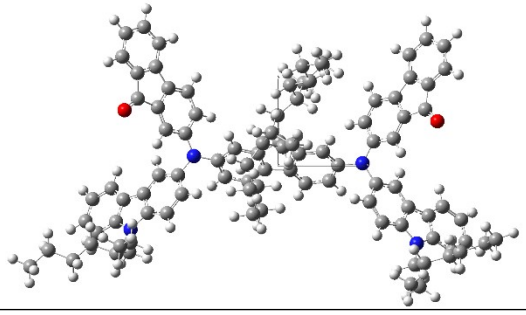	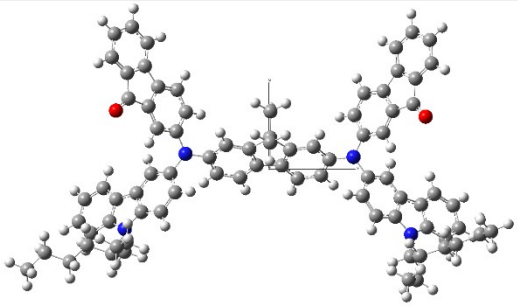
Conformer	V1457b	V1458b

Fig. S21. V1457 and **V1458** compounds. Molecular structure of two conformers in xy projection after ground state energy optimization routine using *Gaussian16*, CAM-B3LYP/6-31G(d,p) basis set.

xy	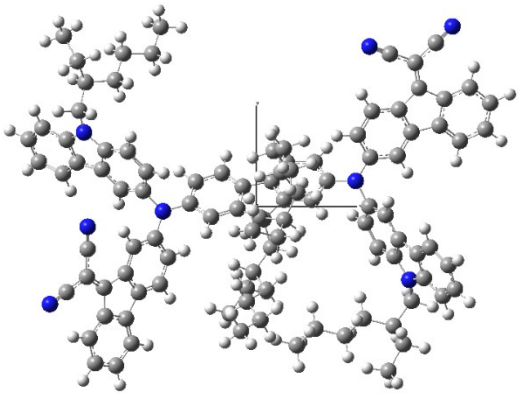	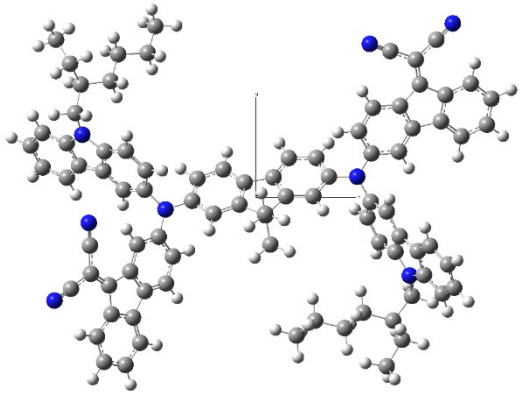
Conformer	V1484a	V1485a
xy	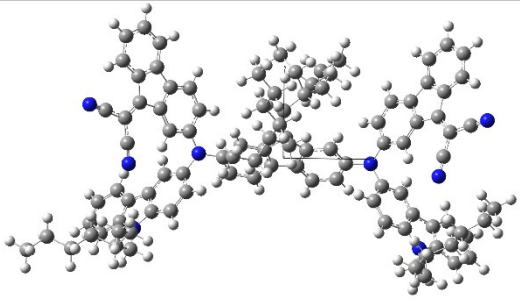	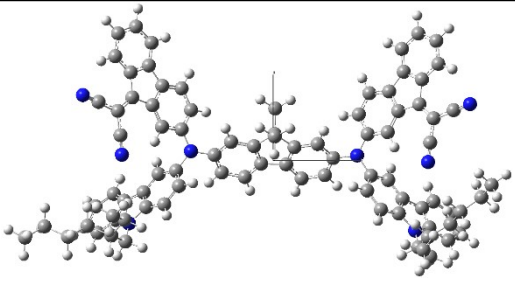
Conformer	V1484b	V1485b

Fig. S22. V1484 and **V1485** compounds. Molecular structure of two conformers in xy projection after ground state energy optimization routine using *Gaussian16*, CAM-B3LYP/6-31G(d,p) basis set.

Table S2. Parameters of electronic excitations (transition energy ΔE_n and corresponding oscillator strength f_n) simulated using semiempirical TD method (for singlets). All allowed transitions for most common conformers are presented in bold.

Compound	$\Delta E_1(S_0 \rightarrow S_1)$, eV	f_1	$\Delta E_2(S_0 \rightarrow S_2)$, eV	f_2	$\Delta E_3(S_0 \rightarrow S_3)$, eV	f_3
V1421a	**3.039**	**0.5513**	3.086	0.0143	3.387	0.0040
V1421b	**3.038**	**0.2336**	**3.096**	**0.3004**	3.387	0.0019
V1421c	3.042	0.2415	3.100	0.3137	3.387	0.0021
V1458a	**2.959**	**0.1301**	**3.275**	**0.3957**	3.439	0.0010
V1458b	**2.939**	**0.1019**	**2.966**	**0.1189**	3.441	0.0035
V1458c	2.943	0.1056	2.970	0.1241	3.439	0.0037
V1485a	2.263	0.0456	**2.679**	**0.4452**	**3.376**	**0.3641**
V1485b	2.210	0.0335	2.225	0.0394	3.303	0.0406
V1485c	2.236	0.0334	2.246	0.0489	3.334	0.0672
V1393a	**3.078**	**0.4650**	3.109	0.0476	3.388	0.0031
V1393b	**3.032**	**0.2188**	**3.132**	**0.2459**	3.385	0.0022
V1393c	2.922	0.1128	2.959	0.2482	3.294	0.0025
V1393d	3.021	0.5256	3.065	0.0103	3.387	0.0022
V1457a	**2.987**	**0.1019**	**3.302**	**0.3603**	3.441	0.0007
V1457b	2.942	0.0890	**2.966**	**0.1140**	3.441	0.0031
V1457c	2.945	0.0923	2.971	0.1187	3.439	0.0031
V1457d	2.994	0.1002	3.295	0.3581	3.442	0.0007
V1484a	2.254	0.0429	**2.677**	**0.4393**	**3.374**	**0.3596**
V1484b	2.217	0.0290	2.231	0.0356	3.311	0.0251
V1484c	2.237	0.0313	2.249	0.0438	3.335	0.0436
V1484d	2.249	0.0433	2.649	0.4538	3.341	0.3744

Electronic excitations were simulated using semiempirical TD method (for singlets). The parameters of transition between MO which are related to the population of "spectroscopic" state are presented in **Table S3**. Spatial distribution of electron density for the HOMO-1, HOMO, LUMO and LUMO+1 is presented in the **Tables S4, S5, S6**.

Table S3. Parameters of electronic excitations simulated using semiempirical TD method (for singlets). Population of "spectroscopic" states (from ground to excited) ΔE_n and corresponding set of MO with contribution coefficient k (contribution of the respective excitation to the configurational interaction wavefunction).

	a conformer			b conformer		
V1421	ΔE	Transition between MO	k	ΔE	Transition between MO	k
	$S_0 \rightarrow S_1$	HOMO→LUMO	0.54548	$S_0 \rightarrow S_1$	HOMO→LUMO	0.54742
	$S_0 \rightarrow S_2$	HOMO→LUMO+1	0.53391	$S_0 \rightarrow S_2$	HOMO→LUMO+1	0.53376
V1393	ΔE	Transition between MO	k	ΔE	Transition between MO	k
	$S_0 \rightarrow S_1$	HOMO→LUMO	0.41500	$S_0 \rightarrow S_1$	HOMO→LUMO	0.54168
	$S_0 \rightarrow S_2$	HOMO→LUMO+1	0.42353	$S_0 \rightarrow S_2$	HOMO→LUMO+1	0.49285
V1458	ΔE	Transition between MO	k	ΔE	Transition between MO	k
	$S_0 \rightarrow S_1$	HOMO→LUMO	0.54776	$S_0 \rightarrow S_1$	HOMO→LUMO	0.50733
	$S_0 \rightarrow S_2$	HOMO→LUMO+1	0.43698	$S_0 \rightarrow S_2$	HOMO-1→LUMO	0.49249

V1457	ΔE	Transition between MO	k	ΔE	Transition between MO	k
	$S_0 \rightarrow S_1$	HOMO→LUMO	0.56039	$S_0 \rightarrow S_1$	HOMO→LUMO	0.48402
	$S_0 \rightarrow S_2$	HOMO-1→LUMO+1	0.45642	$S_0 \rightarrow S_2$	HOMO→LUMO+1	0.47076
V1485	ΔE	Transition between MO	k	ΔE	Transition between MO	k
	$S_0 \rightarrow S_1$	HOMO→LUMO	0.57764	$S_0 \rightarrow S_1$	HOMO→LUMO	0.51457
	$S_0 \rightarrow S_2$	HOMO-1→LUMO+1	0.43269	$S_0 \rightarrow S_2$	HOMO→LUMO+1	0.50820
		HOMO→LUMO+1	-0.42437			
V1484	ΔE	Transition between MO	k	ΔE	Transition between MO	k
	$S_0 \rightarrow S_1$	HOMO→LUMO	0.58658	$S_0 \rightarrow S_1$	HOMO→LUMO+1	0.48290
	$S_0 \rightarrow S_2$	HOMO-1→LUMO+1	0.45292	$S_0 \rightarrow S_2$	HOMO→LUMO	0.45709

Table S4. Compounds **V1421** and **V1393**. Set of MO involved into "spectroscopic" states $S_0 \rightarrow S_1$ and $S_0 \rightarrow S_2$

MO	V1421a	V1421b	V1393a	V1393b
LUMO+1	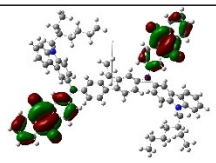	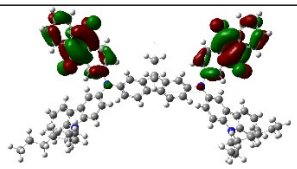	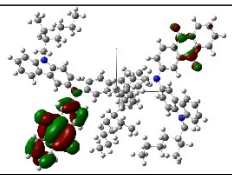	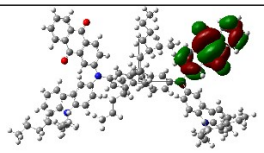
LUMO	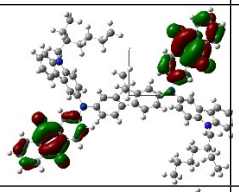	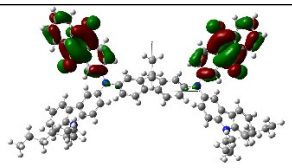	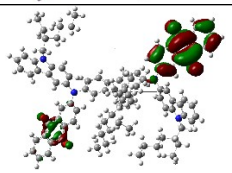	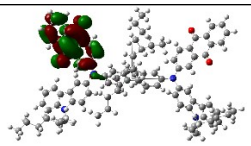
HOMO	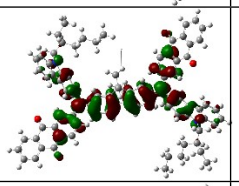	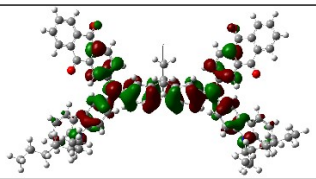	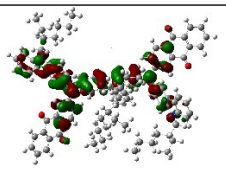	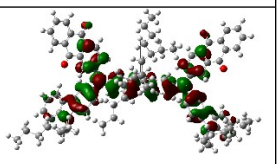
HOMO-1	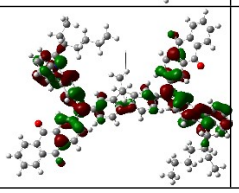	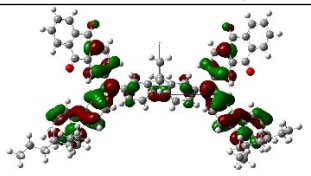	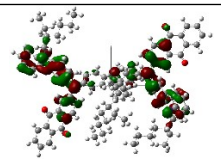	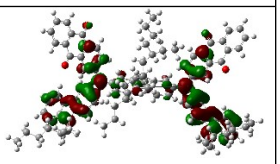

Table S5. Compounds **V1458** and **V1457**. Set of MO involved into "spectroscopic" states $S_0 \rightarrow S_1$ and $S_0 \rightarrow S_2$

MO	V1458a	V1458b	V1457a	V1457b
LUMO+1	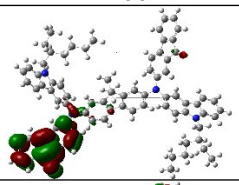	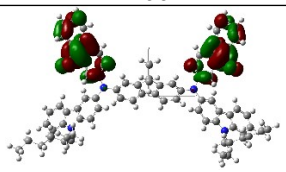	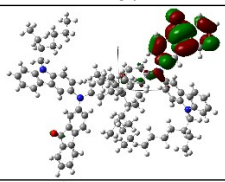	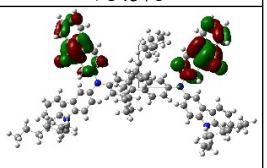
LUMO	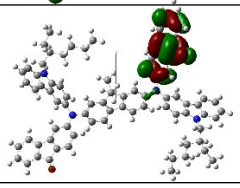	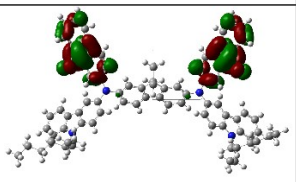	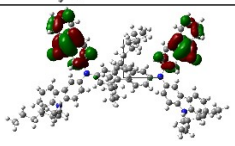	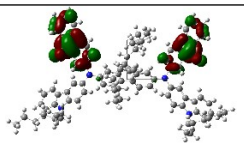

HOMO	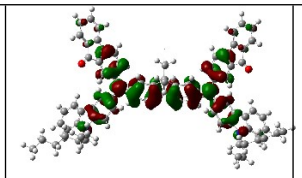	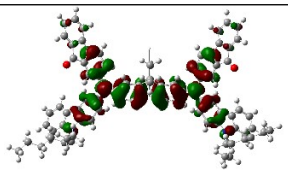	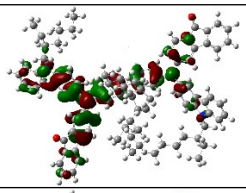	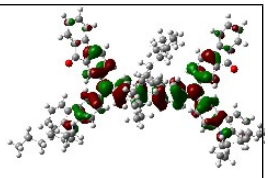
HOMO-1	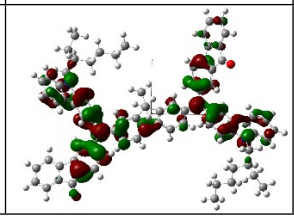	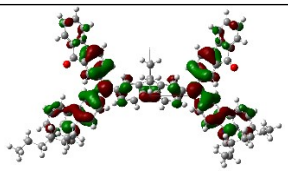	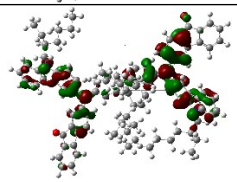	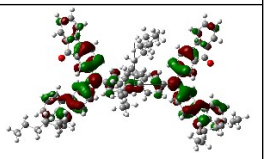

Table S6. Compounds **V1485** and **V1484**. Set of MO involved into "spectroscopic" states $S_0 \rightarrow S_1$ and $S_0 \rightarrow S_2$

MO	V1485a	V1485b	V1484a	V1484b
LUMO+1	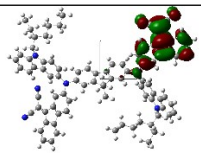	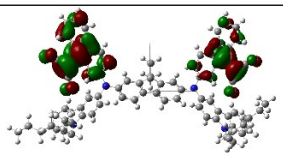	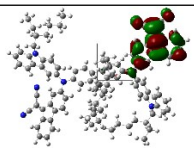	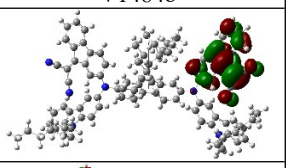
LUMO	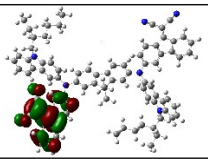	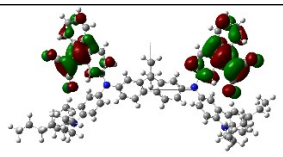	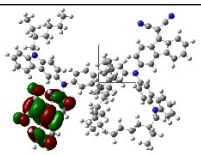	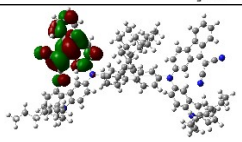
HOMO	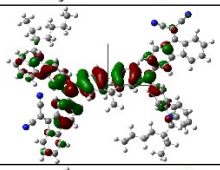	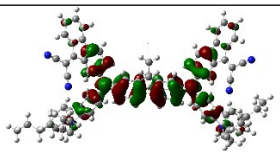	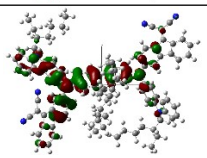	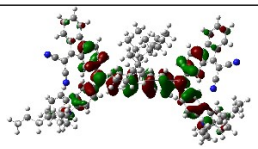
HOMO-1	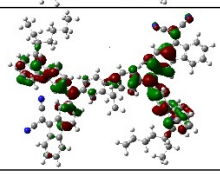	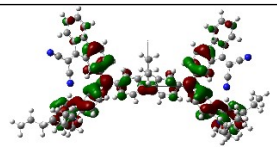	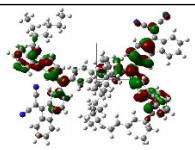	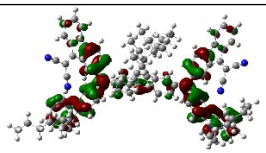

Tables S7, S8, S9 represent HOMO and LUMO NTO (which correspond the electronic densities of hole and electron NTO pairs) for allowed first transition.

Table S7. Compound **V1421**. Set of MO involved into "spectroscopic" states $S_0 \rightarrow S_1$. Electronic densities of hole and electron NTO pairs for allowed transition.

MO	V1421a	V1421b
LUMO	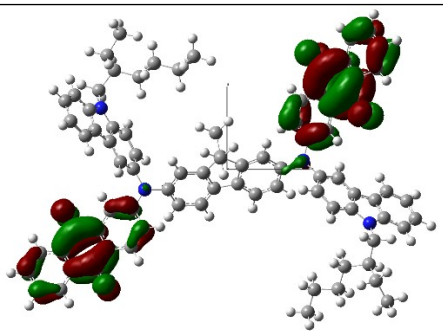	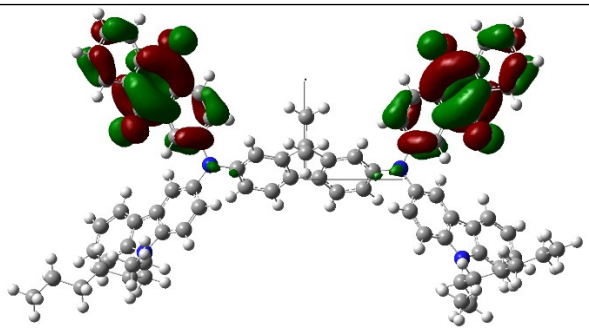
HOMO	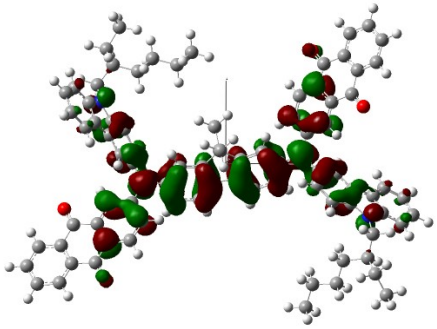	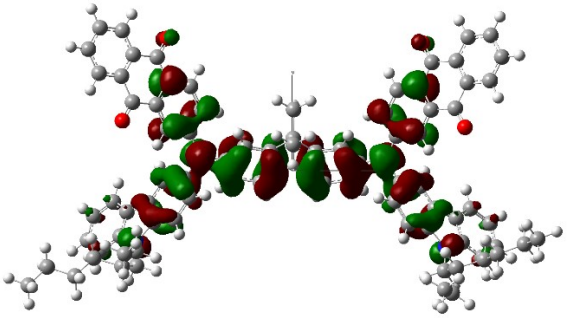

Table S8. Compound **V1458**. Set of MO involved into "spectroscopic" states $S_0 \rightarrow S_1$. Electronic densities of hole and electron NTO pairs for allowed transition.

MO	V1458a	V1458b
LUMO	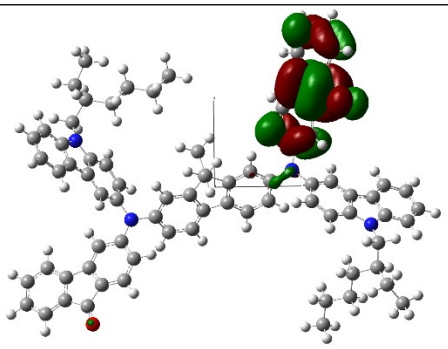	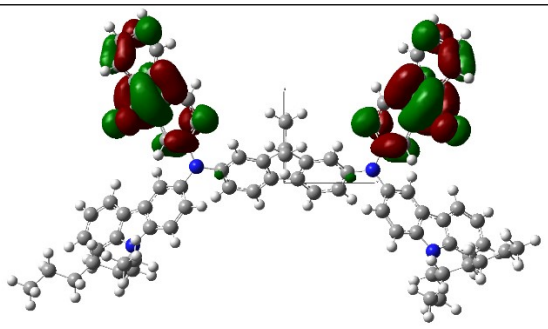
HOMO	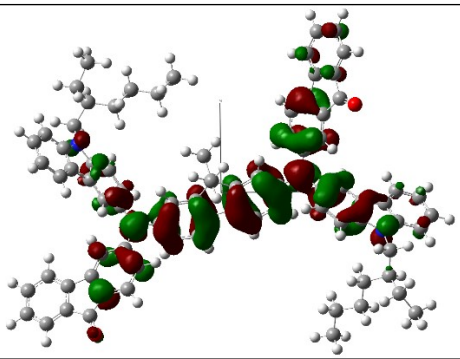	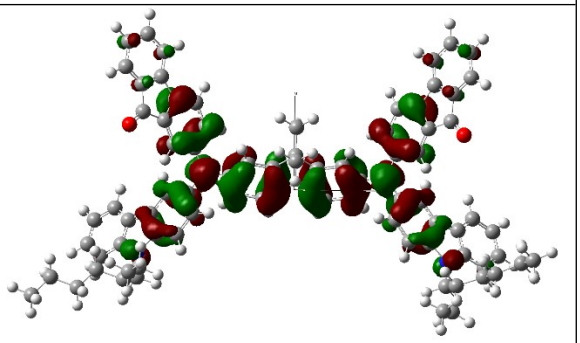

Table S9. Compound **V1485**. Set of MO involved into "spectroscopic" states $S_0 \rightarrow S_1$. Electronic densities of hole and electron NTO pairs for allowed transition.

MO	V1485a	V1485b
LUMO	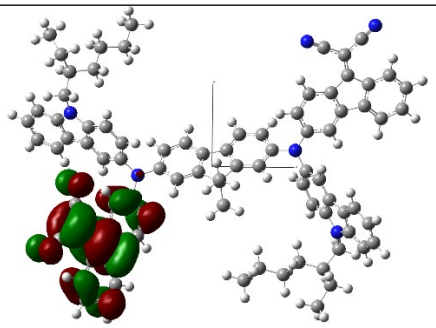	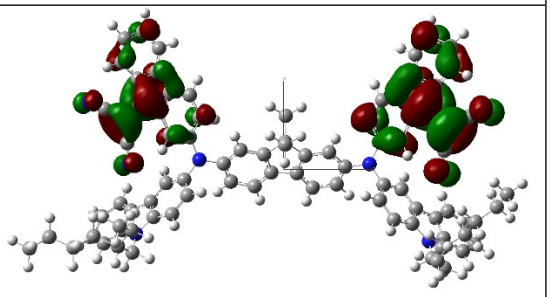
HOMO	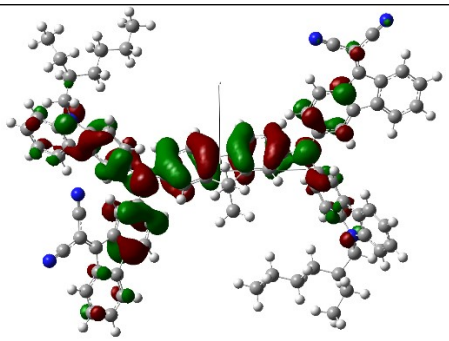	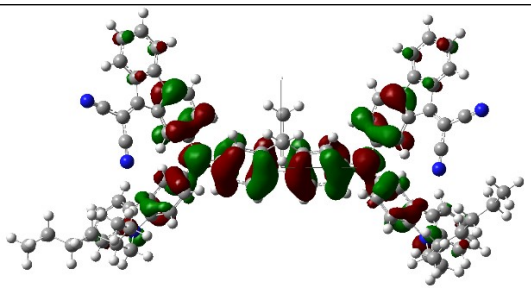

Simulations of ground state molecular structure for several most probable dimers consisting of previously described monomers were carried out using *Gaussian16* software by means of density functional (DFT) CAM-B3LYP method and 6-31G(d,p) basis set supplemented with polarization functions (d,p). List of several most probable molecular dimers is presented in **Table S10**. One several most informative projections (not xy) of the mentioned conformations are presented in **Fig.S5**. Those structures were obtained using grad optimization technique (convergence of parameters Maximum Force, RMS Force, Maximum Displacement, RMS Displacement has been achieved). Electronic excitations were simulated using semiempirical TD method (for singlets).

Table S10. List of molecular dimers.

Compound	Two initial conformers	Molecular structure after ground state energy optimization using *Gaussian16*, CAM-B3LYP/6-31G(d,p) basis set
Eh0	V1421b + V1421b	Fig. S5
Eh2	V1458b + V1458b	Fig. S5

Projection1	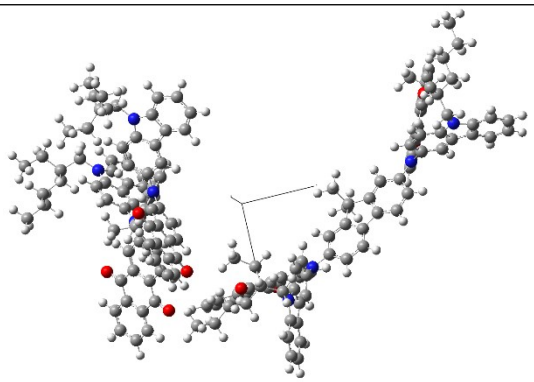	
Projection2	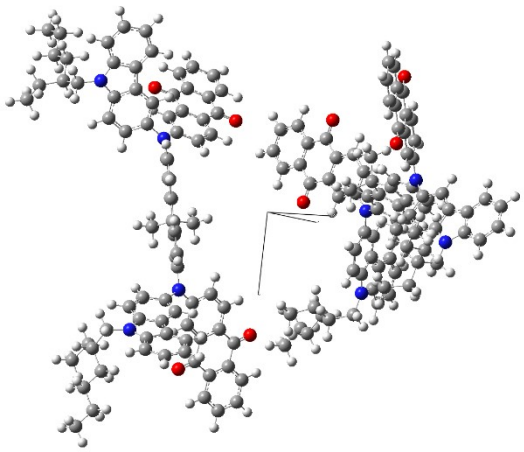	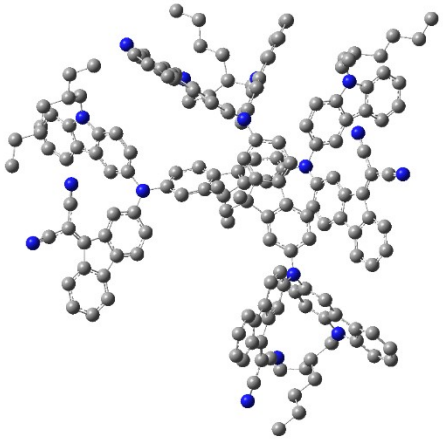
Dimer	**Eh0 (**V1421b + V1421b**)**	**Eh2 (**V1458b + V1458b**)**

Fig. S23. Dimers Eh0 and Eh2. Molecular structure after ground state energy optimization routine using *Gaussian16*, CAM-B3LYP/6-31G(d,p) basis set. Due to best visualization, Eh2 structure presented in style "hydrogens absent"

Optical measurements

Absorption spectra of the synthesized compounds were measured in dilute solutions in THF (concentration $1 \cdot 10^{-4}$ M) and on glass substrate using a UV/Vis–NIR spectrophotometer, Lambda 35 (Perkin–Elmer). The layer thickness of the solution is $d = 1$ mm. Diffraction grating crack width 2 nm. Spectral recording speed 2 nm/s. The wavelength λ is given in nm.

Hole Drift Mobility Measurements

Carrier drift mobility was determined by the time-of-flight (XTOF) method. The material solution (THF) was poured onto aluminum-coated glass plates. The sample was poured from a solution of pure substance. The layers were dried for 1 h at 60 ° C. The thickness of the transport layer was measured with an optical microscope-interferometer. The drift mobility of electron holes (μ) was determined in electrophotographic mode at an electric field of $(0.1 \div 1) \cdot 10^6$

V/cm. Charge carriers were generated at the layer surface by illumination with nitrogen laser nanosecond pulses (λ = 337 nm). Holes or electrons transit time was determined by the kink on the curve of the dU/dt transient in double logarithmic scale.

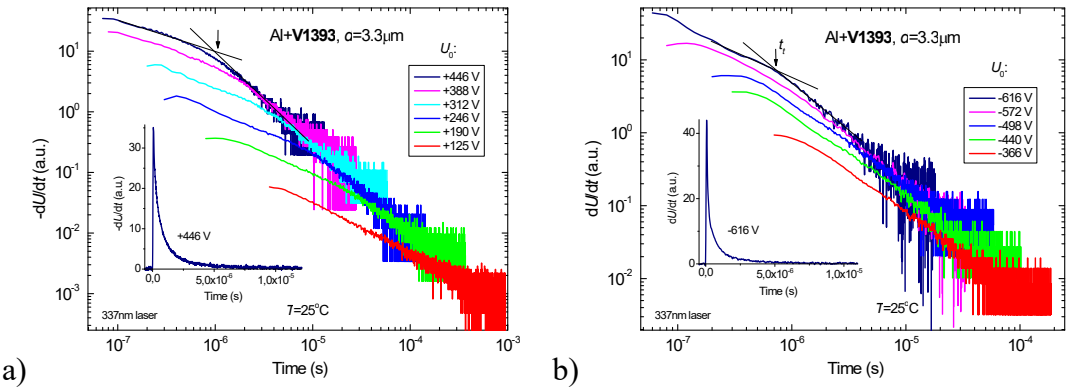

a) b)

Figure S24. XTOF transients in **V1393** sample of holes (a) and electrons (b).

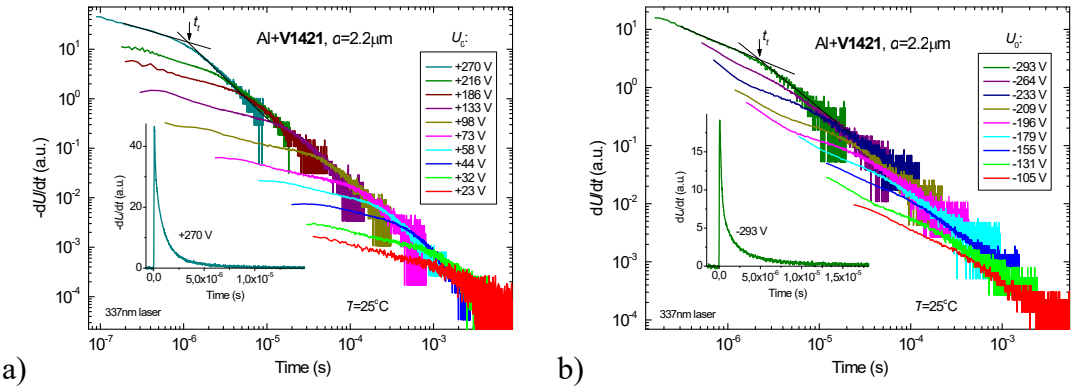

a) b)

Figure S25. XTOF transients in **V1421** sample of holes (a) and electrons (b).

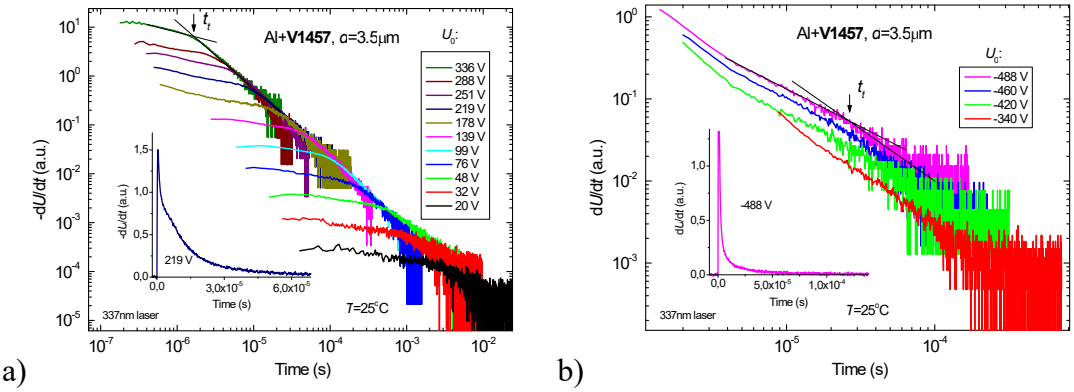

a) b)

Figure S26. XTOF transients in **V1457** sample of holes (a) and electrons (b).

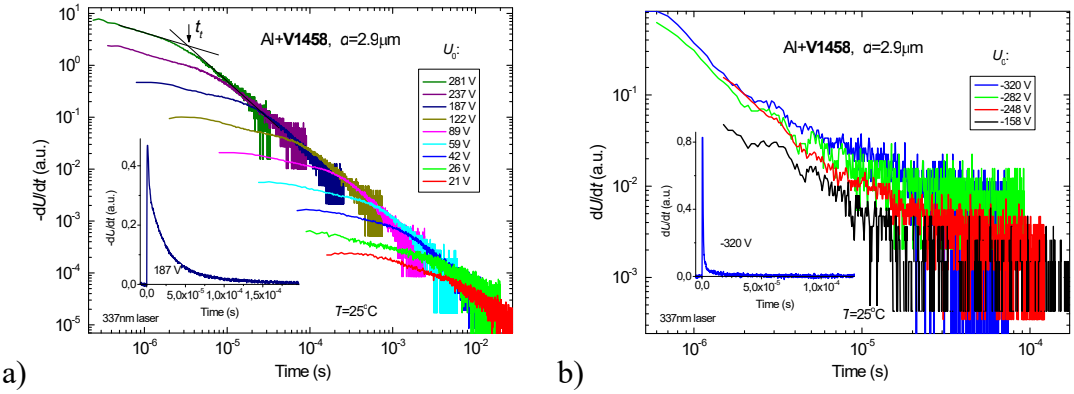

a) b)

Figure S27. XTOF transients in **V1458** sample of holes (a) and electrons (b).

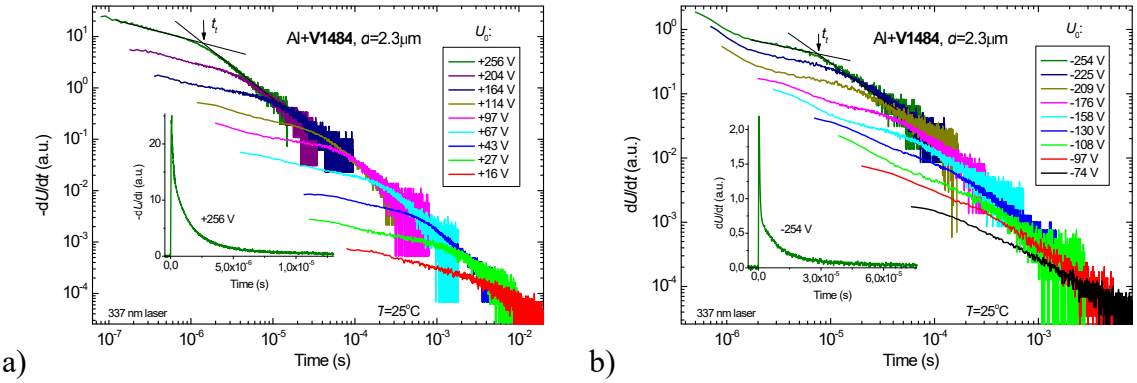

a) b)

Figure S28. XTOF transients in **V1484** sample of holes (a) and electrons (b).

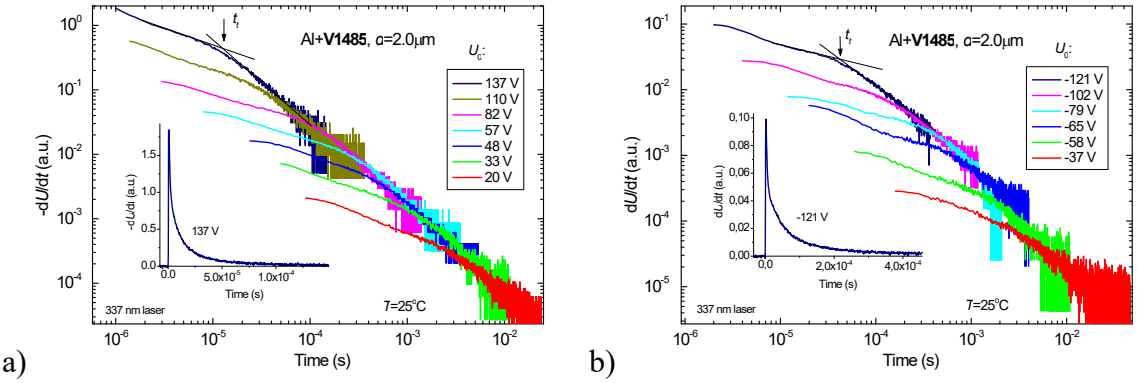

a) b)

Figure S29. XTOF transients in **V1485** sample of holes (a) and electrons (b).

Photocurrent decay study

Conditions: excitation wavelength λ = 355 nm, pulse duration a few ns, surface absorption (αd=3.5-6).

Photocurrent decays were observed over a wide range: starting from 1 μs to several ms while changing the load resistance. Photocurrent decay kinetics: normalized to unity. Connected electric field: less than the field required to extract carriers from the sample (about 60 kV/cm),

therefore the decrease in photocurrent was mainly due to recombination and carrier trapping. Type of carriers observed: changed by changing the polarity of the applied voltage.

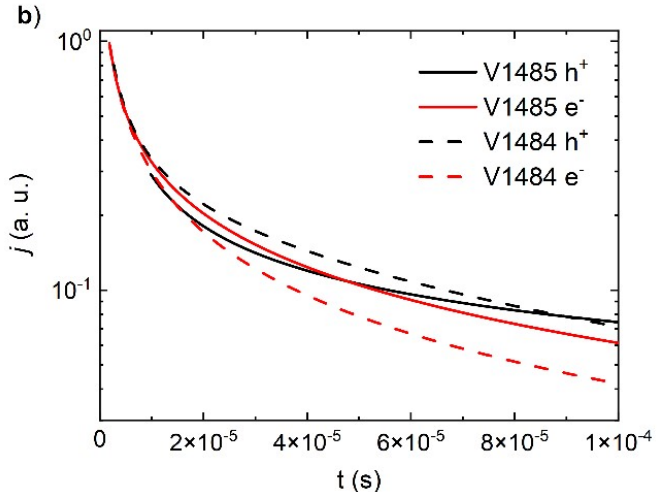

Figure S30. Photocurrent decay profile of compound film containing cyanoylidene fragments (**V1393** and **V1421**).

Conductivity measurements

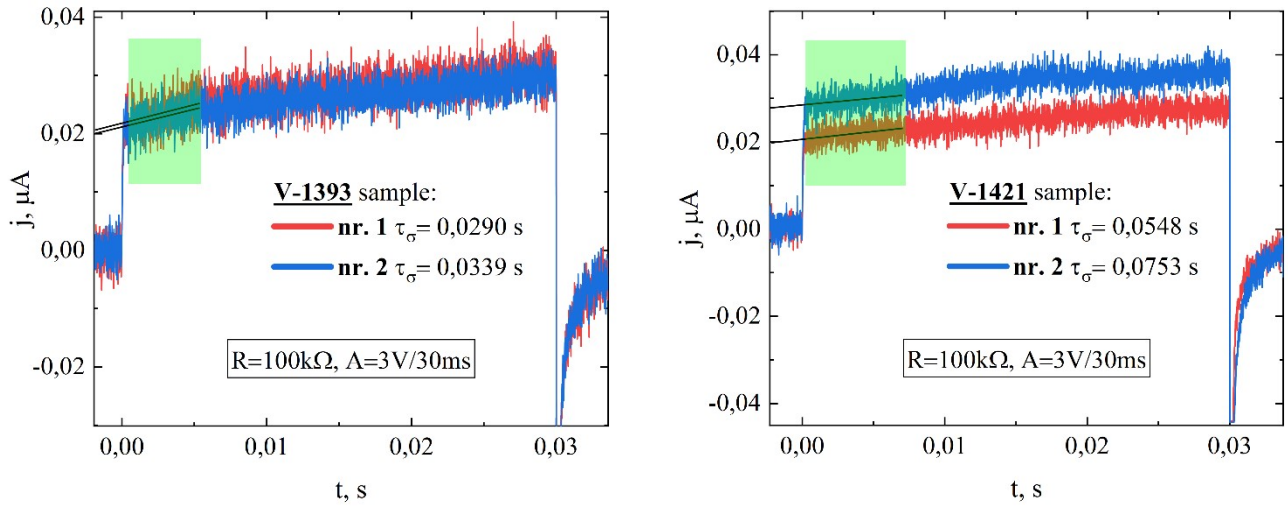

Figure S31. V1393 and **V1421** CELIV transients for conductivity measurement

Conductivity assessment was performed via the Charge Extraction by Linearly Increasing Voltage (CELIV) technique [6]. In this method, a linearly rising reverse bias voltage was applied to the sample, and subsequently, charge extraction transients were recorded. The

determination of conductivity values involved fitting the initial ascent in the transient response curve and extracting the relaxation time τ_σ, as depicted in **Figure S31**. Detailed conductivity values can be found in **Table S7** for reference.

Table S11. Conductivities of all compound films.

Compound	τ_σ**, s**	**σ, 1·10^{-12}S·cm^{-1}**
V-1393	0,031	9,910
V-1421	0,065	4,884
V-1457	0,047	6,595
V-1458	0,020	16,40
V-1484	0,044	6,992
V-1485	0,013	2,487

References

[1] A. Midya, Z. Xie, J. X. Yang, Z. K. Chen, D. J. Blackwood, J. Wang, S. Adams, K. P. Loh, *Chem. Commun.*, **2010**, *46*, 2091.

[2] J. Nekrasovas, V. Gaidelis, E. Kamarauskas, M. Viliunas, V. Jankauskas, *J. Appl. Phys.* **2019**, *126*, DOI 10.1063/1.5096070.

[3] A. Paul, R. Borrelli, H. Bouyanfif, S. Gottis, F. Sauvage**,** *ACS Omega* **2019**, *4, 12*, 14780.

[4] V. V. Pavlishchuk, A. W. Addison, *Inorganica Chimica Acta*, **2000**, *298*, 97–102.

[5] H. Reiss and A. Heller, *J. Phys. Chem.* **1985**, *89*, 4207–4213.

[6] Juška, G. & Arlauskas, Kestutis & Viliunas, M & Kočka, J. (2000). Extraction Current Transients: New Method of Study of Charge Transport in Microcrystalline Silicon. Physical review letters. 84. 4946-9. 10.1103/PhysRevLett.84.4946.